Available online at www.sciencedirect.com
ScienceDirect
Journal of Nuclear Materials 366 (2007) 137–160
journal of nuclear materials
www.elsevier.com/locate/jnucmat

Preparation and characterization of $(Ba,Cs)(M,Ti)_8O_{16}$ ($M = Al^{3+}$, Fe^{3+}, Ga^{3+}, Cr^{3+}, Sc^{3+}, Mg^{2+}) hollandite ceramics developed for radioactive cesium immobilization

V. Aubin-Chevaldonnet [a], D. Caurant [a,*], A. Dannoux [a], D. Gourier [a], T. Charpentier [b], L. Mazerolles [c], T. Advocat [d]

[a] *CNRS, Ecole Nationale Supérieure de Chimie de Paris (ENSCP, Paristech), Laboratoire de Chimie de la Matière Condensée de Paris (UMR-CNRS 7574), 11 rue Pierre et Marie Curie, 75231 Paris cedex 05, France*
[b] *Commissariat à l'Energie Atomique Saclay, Laboratoire de Structure et Dynamique par Résonance Magnétique, DSM/DRECAM/SCM-CEA/CNRS URA 331, 91191 Gif sur Yvette, France*
[c] *Centre d'Etudes de Chimie Métallurgique (UPR 2801), 15 Rue Georges Urbain, 94407 Vitry-sur-Seine, France*
[d] *Commissariat à l'Energie Atomique Marcoule, Laboratoire d'Etude de Base sur les Verres, 30207 Bagnols-sur-Cèze, France*

Received 7 July 2006; accepted 15 December 2006

Abstract

Among the different matrices proposed for selective and durable immobilization of radioactive cesium, $(Ba_x,Cs_y)(M,Ti)_8O_{16}$ hollandite ceramics, with $x + y < 2$ and M = divalent or trivalent cation appeared as the best candidates. In this study, hollandite ceramics were prepared using oxide route from oxide, carbonate and nitrate powders with and without Cs for different cations M (Al^{3+}, Cr^{3+}, Ga^{3+}, Fe^{3+}, Mg^{2+}, Sc^{3+}) of increasing size, in order to evaluate the effect of composition on ceramics microstructure and structure and on cesium incorporation. To reduce the risks of Cs vaporization during synthesis, calcined powders were sintered in air at moderate temperature (1200 °C). This oxide route appeared as an alternative to the alkoxide route generally proposed to prepare hollandite waste form. For $y = 0$, single phase $Ba_x(M,Ti)_8O_{16}$ was obtained only for $M^{3+} = Al^{3+}$, Cr^{3+} and Fe^{3+}. For $y \neq 0$ and Fe^{3+}, all cesium was incorporated in hollandite and ceramic was well densified. For Cr^{3+} and Ga^{3+}, only 46% and 63%, respectively, of Cs were retained in hollandite phase. For these samples, a high fraction of Cs was either evaporated and/or concentrated in a Cs-rich parasitic phase. Mixed hollandite samples with $M^{3+} = Ga^{3+} + Al^{3+}$ and $M^{3+} = Fe^{3+} + Al^{3+}$ were also synthesized and the best results regarding Cs immobilization and ceramic density were obtained with iron + aluminum but the sample porosity was higher than that of the sample containing only iron. All results were discussed by considering cations size and refractory character of oxides and hollandite ceramics.

PACS: 81.05.Je; 81.05.Mh; 81.20.Ev; 68.37.Hk; 61.10.Nz

* Corresponding author. Tel.: +33 1 44 27 67 08; fax: +33 1 46 34 74 89.
E-mail address: daniel-caurant@enscp.fr (D. Caurant).

0022-3115/$ - see front matter © 2007 Elsevier B.V. All rights reserved.
doi:10.1016/j.jnucmat.2006.12.051

1. Introduction

Several countries reprocess their civil nuclear spent fuel in order to recover U and Pu for reuse using the Purex process. The high level radioactive liquid wastes (HLW) produced during this reprocessing are made of a complex mixture of both radioactive (fission products, minor actinides) and non-radioactive elements. After evaporation and calcination, these wastes are currently immobilized in borosilicate glasses [1]. Due to the lack of long range order in glassy matrices, glasses remain the best waste forms for immobilization of complex waste mixtures. During the first centuries of waste containers disposal in deep repositories, radioactivity and potential radiotoxicity will be mainly controlled by short-lived radionuclides (^{137}Cs, ^{90}Sr) and then by long-lived minor actinides (MA: Np, Am, Cm) and long-lived fission products [2,3]. In order to minimize the potential long-term impact of HLW, studies are in progress in France on enhanced chemical separation processes of long-lived radionuclides such as MA and ^{135}Cs (half life 2.3×10^6 years) [4]. Two options are then envisaged for these separated radionuclides: (i) transmutation into short-lived or non-radioactive elements, (ii) incorporation in very highly durable matrices.

^{135}Cs approximately represents 14% of all the cesium isotopes in UO_2 spent fuel [5] and selective separation methods using functionalized calixarene molecules are under development to isolate cesium from HLW [6]. As transmutation of ^{135}Cs cannot be envisaged without isotopic separation [7], it is proposed to immobilize all cesium isotopes (^{133}Cs, ^{134}Cs, ^{135}Cs and ^{137}Cs) in ceramic matrices more durable than current nuclear glasses. It can be notice that in France, the amount of ^{135}Cs generated every year after spent fuel reprocessing is about 390 kg which represents nearly 35 wt% of the total amount of MA (1099 kg) generated during the same period [5]. The selective immobilization of cesium in a specific highly durable matrix would reduce the risks of ^{135}Cs migration towards biosphere. Indeed, as cesium is an alkaline element, it is among the most mobile elements if nuclear glass alteration by aqueous media occurred during disposal.

Different kinds of ceramic matrices were proposed as specific waste forms for Cs immobilization such as: pollucite ($CsAlSi_2O_6$) [8], CsZP ($CsZr_2(PO_4)_3$) [9], Synroc-type barium hollandite ($(Ba_xCs_y)[(Ti,Al)^{3+}_{2x+y}Ti^{4+}_{8-2x-y}]O_{16}(x+y<2)$) [10] and iron-rich barium hollandite ($(Ba_xCs_y)[(Fe,Al)^{3+}_{2x+y}Ti^{4+}_{8-2x-y}]O_{16}(x+y<2)$) [11]. Considering both the possibility to prepare well densified hollandite samples, the ability of this matrix to incorporate both Cs^+ and Ba^{2+} ions (barium results from the β-decay of cesium radioactive isotopes) and the occurrence of Ti^{4+} ions in the structure that can act as electron traps during β-decay ($Ti^{4+} + e^-(\beta^-) \rightarrow Ti^{3+}$), hollandite-type matrices appear today as the best candidates for cesium immobilization in comparison with silicate and phosphate ceramic matrices. Indeed, literature indicated that it was difficult to obtain single-phase pollucite samples with high density [12]. Moreover, none of the cations of pollucite (Al^{3+}, Si^{4+}) can act as electron trap during β-decay. Concerning CZP, for which only a small number of studies were performed, a fraction of Zr^{4+} ions can probably be reduced to Zr^{3+} ions under β-decay but the ability of this matrix to incorporate Ba^{2+} ions was not demonstrated to the best of our knowledge. Moreover, it is important to point out that hollandite was also shown to be able to incorporate Rb^+ and Sr^{2+} ions in its structure [13]. Rb is a fission product that represents less than 10 wt% of all Cs in HLW and Sr is the decay product of radioactive Rb. As Cs^+ and Rb^+ both alkali ions show similar chemical properties, they will be co-extracted from HLW during cesium separation process [14]. It is thus important that the selected waste form accepts simultaneously Cs^+, Ba^{2+}, Rb^+ and Sr^{2+} ions in its structure, which is the case within the tunnels of hollandite structure (Fig. 1).

Historically, barium hollandite (nominally $BaAl_2Ti_6O_{16}$) was initially envisaged in the Synroc ceramics developed by Ringwood and coworkers in Australia in the 1970s for the immobilization of Purex-type HLW [15–17]. Synroc waste form consisted of an assemblage of four main titanate crystalline phases able to incorporate in their structure nearly all the elements present in HLW: hollandite (for Cs, Ba and Rb immobilization), zirconolite (nominally $CaZrTi_2O_7$, for lanthanides, actinides and Zr immobilization), perovskite (nominally $CaTiO_3$, for Sr, lanthanides and actinides immobilization) and non-stoichiometric titanium oxides Ti_nO_{2n-1}. In order to achieve a high degree of homogeneity and a high reactivity of precursors before heat treatments, Synroc samples were prepared by mixing and hot-pressing the calcined HLW with titanium, zirconium, aluminum, barium and calcium hydroxides or alkoxides. To control the redox state of multivalent elements (Ti, Mo, ...), a small quantity of titanium metal was added to the

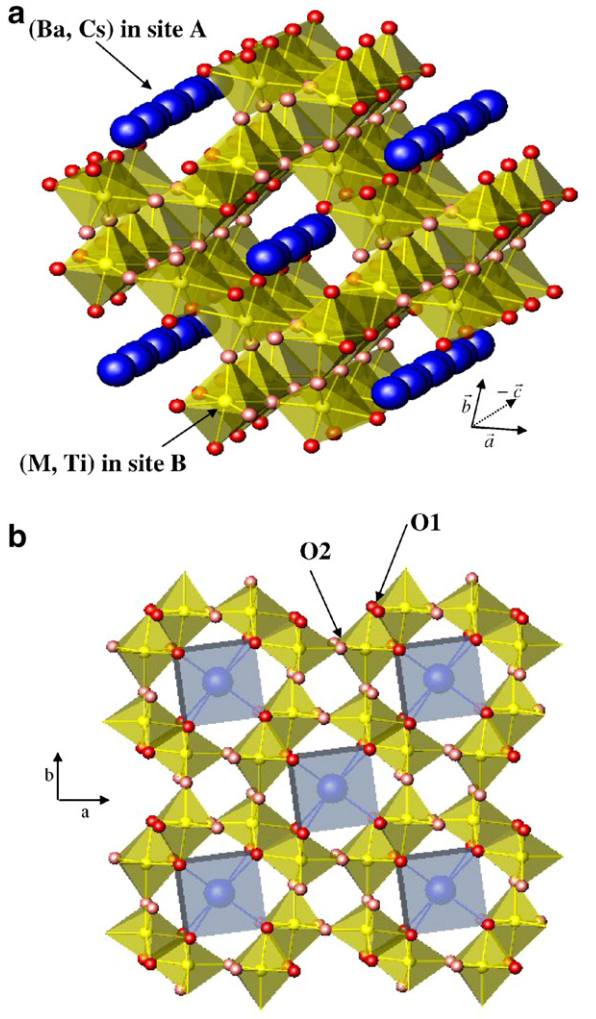

Fig. 1. View of the $(Ba_xCs_y)(M^{3+}_{2x+y}Ti^{4+}_{8-2x-y})O_{16}$ hollandite structure (a) perspective view showing how large cations (Ba^{2+}, Cs^{+}) are incorporated in tunnels (site A) in the framework of $(M,Ti)O_6$ octahedra (site B), (b) projection along the *c*-axis, M: trivalent or divalent cation. In this figure, the *c*-axis is directed along the tunnels which corresponds to the tetragonal ($a = b$) structure of hollandite (for the monoclinic structure the tunnel direction corresponds to *b*-axis). As $(x + y) < 2$, site A (box-shaped cavities of eight oxygen ions) is not totally occupied. The effect of large cations in site B is to enlarge the tunnel cavities (site A): this facilitates inclusion of Cs^{+} ions into the structure. The two kinds of oxygen sites (O1 and O2) occurring in hollandite tetragonal structure (I4/m space group) are also shown.

mixture. This induced partial reduction of Ti^{4+} ions in Ti^{3+} ions in the octahedral sites of the barium hollandite phase thus facilitating incorporation of the big Cs^{+} ions (Table 1) in tunnels of the structure (see next paragraph and Fig. 1). Indeed, because of the small size of Al^{3+} ions (Table 1), it was very difficult to incorporate significant amounts of cesium in the hollandite structure without partially reducing titanium [10]. After Cs incorporation and partial reduction of titanium, Synroc hollandite had the following composition: $(Ba_xCs_y)[(Ti,Al)^{3+}_{2x+y}\text{-}Ti^{4+}_{8-2x-y}]O_{16}(x + y < 2)$ [18]. Chemical durability tests performed on single phase Synroc hollandite showed its very good resistance to water attack over the pH range 2–13 [19]. Concerning the behavior of barium hollandite under β-decay, a simple Ba-hollandite composition prepared under air and without cesium ($Ba_{1.16}Al_{2.32}Ti_{5.68}O_{16}$) was recently studied by Electron Paramagnetic Resonance (EPR) after external electron irradiation with a Van de Graff accelerator simulating cesium β self-irradiation [20–22]. Small concentrations of electron and hole centers were detected and their stability was followed with increasing annealing temperature *T*. An aggregation phenomena of hole centers was observed on increasing *T* but this phenomena had probably no significant effect on hollandite long term behavior.

Recently, an iron-rich single phase mixed (Ba,Cs, Al + Fe)-hollandite[1] $(Ba_xCs_y)[(Fe,Al)^{3+}_{2x+y}Ti^{4+}_{8-2x-y}]O_{16}$ ceramic with $x = 1$ and $y = 0.28$ that could be easily prepared under air, was proposed as specific waste form for radioactive cesium immobilization [11]. By introducing iron in hollandite composition, it was not necessary to prepare the samples under reducing conditions as for Synroc-hollandite. After sintering under air, iron ions occurred mainly as Fe^{3+} ions in hollandite as demonstrated by Mössbauer spectroscopy [23]. As ferric ions have ionic radius only slightly smaller than Ti^{3+} ions (Table 1), they would also facilitate Cs^{+} ions incorporation in the tunnels of the structure (see next paragraph and Fig. 1). Alteration tests by water showed that the chemical durability of $(Ba_xCs_y)\text{-}[(Fe,Al)^{3+}_{2x+y}Ti^{4+}_{8-2x-y}]O_{16}$ hollandite was as good as the one of Synroc hollandite [11].

Although several papers [13,18,24] reported the preparation of various hollandite compositions using oxide and carbonate powders mixture as ceramic precursor (this method is referred to as 'oxide route'), the method generally proposed in literature to prepare single phase $(Ba_xCs_y)[M^{3+}_{2x+y}Ti^{4+}_{8-2x-y}]O_{16}$ hollandites with $M^{3+} = Ti^{3+} + Al^{3+}$ [10,19,25] or $M^{3+} = Fe^{3+} + Al^{3+}$ [11] used alkoxide, nitrate or acetate precursors in solution as in Synroc

[1] In this paper, $Ba_xCs_y(M,Ti)_8O_{16}$ hollandite samples are referred to as (Ba,Cs,M)-hollandite.

Table 1
Ionic radius of cations M = Al^{3+}, Cr^{3+}, Ga^{3+}, Fe^{3+}, Ti^{3+}, Mg^{2+}, Sc^{3+} in sixfold coordination (octahedral site B in hollandite) and of cations Ba^{2+} and Cs^{+} in eightfold coordination (site A in hollandite) [49] (see Fig. 1)

Cation	Al^{3+}	Cr^{3+}	Ga^{3+}	Fe^{3+}	Ti^{3+}	Mg^{2+}	Sc^{3+}	Ti^{4+}	Ba^{2+}	Cs^{+}
r (Å)	0.535	0.615	0.620	0.645	0.670	0.720	0.745	0.605	1.42	1.74
r_B (Å)	0.585	0.608	0.609	0.616	0.624	0.622	0.645	–	–	–
t_H	1.006	0.991	0.990	0.985	0.980	0.982	0.966	–	–	–

r_B is the average radius of cations in site B of $Ba_{1,16}(M^{3+}_{2.32}Ti_{5.68})O_{16}$ and $Ba_{1.16}(M^{2+}_{1.16}Ti_{6.84})O_{16}$ hollandites. In this table is also reported the radius ratio tolerance factor t_H defined by Kesson and White [45], that can be used to predict the stability of $Ba_{1,16}(M^{3+}_{2.32}Ti_{5.68})O_{16}$ and $Ba_{1.16}(M^{2+}_{1.16}Ti_{6.84})O_{16}$ hollandites for the different cations M. The more stable structures correspond to t_H values close to 1. The calculation of t_H was based on geometrical considerations (the hollandite structure was assumed to be more stable if the big cations Ba^{2+} or Cs^{+} (in site A) fit within the tunnels): $t_H = \frac{[(r_A+r_O)^2-\frac{1}{2}(r_B+r_O)^2]^{\frac{1}{2}}}{\sqrt{\frac{3}{2}}(r_B+r_O)}$ (r_A: average ionic radius of cations in site A, r_O: oxygen ion radius: 1.4 Å).

preparation method (this method is referred to as 'alkoxide route'). For instance, Carter et al. [19] mixed aluminum sec-butoxide and titanium isopropoxide in ethanol with barium and cesium nitrates dissolved in water. After drying, calcination (750 °C) and milling, the samples were hot pressed (1200–1250 °C) in graphite dies. In their method, Bart et al. [11] used the same kind of precursors but ferrous nitrate was added to the aqueous solution.

The aim of the present work was to study the effect of the nature of cation M (trivalent or divalent) introduced in hollandite composition on the ease of preparation of single phase ceramics (containing or not cesium) under air at moderate sintering temperature (1200 °C during 30 h, to limit the risks of Cs vaporization) using an oxide route without hot-pressing. This dry process appeared as an alternative method to the alkoxide route which enables to use cheaper raw materials (oxides, carbonates) than alkoxides (titanium isopropoxide, aluminum sec-butoxide). Moreover, the oxide route avoids the use of a stir drying apparatus needed to remove the solvent present in precursors mixture obtained after reaction between organometallic and aqueous reagents for the alkoxide route.

For this purpose, we first tried to prepare single phase (Ba,M)-hollandite $(Ba_xCs_y)(M,Ti)_8O_{16}$ ceramics without cesium (i.e. $y = 0$) for $x = 1.16$ with cations M (Al^{3+}, Cr^{3+}, Ga^{3+}, Fe^{3+}, Mg^{2+}, Sc^{3+}) of increasing size (Table 1). The compositions were, respectively, $Ba^{2+}_{1.16}(M^{3+}_{2.32}Ti^{4+}_{5.68})O_{16}$ and $Ba^{2+}_{1.16}(M^{2+}_{1.16}Ti^{4+}_{6.84})O_{16}$ for trivalent and divalent cations M. The choice of the same x value ($x = 1.16$) for all the (Ba,M)-hollandite compositions in this work was made according to the domains of existence of single phase hollandite ceramics reported in literature (Table 2). These domains were determined almost exclusively for hollandites without Cs ($y = 0$) and prepared at higher temperature ($T \geqslant 1300$ °C) than in our case. The composition limits reported in Table 2 concerned mainly literature references in which samples were studied by both X-ray diffraction (XRD) and electron microscopy. We did not include in Table 2 references giving domains with $x < 1$ because the single phase character of samples was not checked by electron microscopy: secondary phases may occur that were not detected by XRD and the limits given must be considered with caution. For instance, Sinclair et al. [26] reported that single phase $Ba_x(Al_{2x}Ti_{8-2x})O_{16}$ hollandite extended from $x = 0.3$–1.2 but no electron microscopy results were presented in their paper. However, Zandbergen et al. [13] used both XRD and electron microscopy for various Ba-hollandite compositions to show that single phase hollandites existed only for $x > 1$. The choice of $x = 1.16$ made in the present work was the same as in our previous studies on external electron irradiation of $Ba_{1.16}(Al_{2.32}Ti_{5.68})O_{16}$ hollandite [20–22]. Table 2 indicates that, except for M = Sc, all $Ba_{1.16}(M,Ti)_8O_{16}$ were reported to be single-phase hollandite ceramics. Mixed-hollandite ceramics containing two kinds of trivalent cations M^{3+} ($Al^{3+} + Fe^{3+}$; $Ba_{1.28}(Al_{1.64}Fe_{0.92}Ti_{5.44})O_{16}$) and ($Al^{3+} + Ga^{3+}$; $Ba_{1.28}(Al_{1.64}Ga_{0.92}Ti_{5.44})O_{16}$) were also synthesized.

Table 2
Single-phase domains of composition (x_{min}–x_{max}) of $Ba_x(M,Ti)_8O_{16}$ hollandite ceramics for different cations M according to various literature references indicated in the table

Cations M	Single-phase domains of $Ba_x(M,Ti)_8O_{16}$ (x_{min}–x_{max})	References
Al^{3+}	1.16–1.28	[13,50]
Cr^{3+}	1.12–1.34	[13,50]
Ga^{3+}	1.16–1.32	[13,50]
Fe^{3+}	1.1–1.3	[34]
Mg^{2+}	1.14–1.33	[31,39]
Sc^{3+}	1.18–1.34	[13]

For each of the single phase (Ba,M)-hollandite $Ba_{1.16}(M,Ti)_8O_{16}$ ceramics obtained in this work ($M^{3+} = Cr^{3+}$, Ga^{3+} and Fe^{3+}, see below), we then tried to prepare single phase (Ba,Cs,M)-hollandite $Ba_xCs_y(M,Ti)_8O_{16}$ samples with cesium, keeping the same amount of cations M^{3+} as in the (Ba,M)-hollandite samples (i.e. 2.32 per formula unit). For charge compensation reasons, it was necessary to increase the total amount of cations in the tunnels of the structure. We decided to prepare compositions with $x = 1.04$ and $y = 0.24$ (i.e. $(Ba^{2+}_{1.04}Cs^{+}_{0.24})$-$(M^{3+}_{2.32}Ti^{4+}_{5.68})O_{16}$). This composition ($x + y = 1.28$) was chosen in order to compare our results with the ones obtained by Bart et al. [11] for their $(Ba_{1.00}Cs_{0.28})(Al_{1.46}Fe_{0.82}Ti_{5.72})O_{16}$ hollandite. Unlike Synroc-hollandite and the iron-rich barium hollandite developed by Bart et al. [11], aluminum ions were totally replaced by chromium, gallium, iron, magnesium or scandium in the $Ba_xCs_y(M,Ti)_8O_{16}$ samples prepared for this study. By increasing the size of cation M in octahedral sites, it was aimed at increasing the section of the tunnels in order to facilitate cesium incorporation in the structure (Fig. 1). In order to increase powders mixture reactivity and to reduce the risks of cesium vaporization during thermal treatments, we used in this study the oxide route preparation method we previously optimized for the $(Ba_{1.00}Cs_{0.28})(Al_{1.46}Fe_{0.82}Ti_{5.72})O_{16}$ composition containing both Al^{3+} and Fe^{3+} ions [20,23]. To compare this dry process with the method used by Bart et al. [11] to synthesize mixed (Ba,Cs,Al + Fe)-hollandite, a $(Ba_{1.0}Cs_{0.28})(Al_{1.46}Fe_{0.82}Ti_{5.72})O_{16}$ ceramic sample was also prepared using alkoxide route.

In this work, the microstructure, structure and composition of all hollandite ceramic samples were studied. For the samples containing cesium but no paramagnetic M cations (Fe^{3+},Cr^{3+}), the occurrence of low durability secondary phases able to concentrate cesium was carefully studied using ^{133}Cs MAS-NMR (Magic Angle Spinning-Nuclear Magnetic Resonance). Among the different cations M envisaged to prepare (Ba,Cs,M)-hollandites by oxide route at 1200 °C, it is shown in this work that $M^{3+} = Fe^{3+}$ and $M^{3+} = Fe^{3+} + Al^{3+}$ are the most suitable to prepare waste forms.

2. The structure of (Ba,Cs) titanate hollandite

The (Ba,Cs,M)-titanate hollandite $(Ba_xCs_y)(M,Ti)_8O_{16}$ ($x + y < 2$) type structure is shown in Fig. 1. Approximately square tunnels running parallel to the short axis of the structure are enclosed by columns of two edge-sharing octahedra which then share corners. The small Ti and M cations are located in these octahedral sites (site B). The large Ba^{2+} and Cs^{+} cations are set in the tunnels in box-shaped cavities of eight oxygen ions (site A). In spite of the relatively open-framework-type structure of (Ba,Cs,M)-hollandite, Ba^{2+} and Cs^{+} ions have to overcome a large energy barrier associated with passing through the square planar arrangement of oxygen ions to migrate along the axis of the tunnels and these compounds appeared as very bad ionic conductors [23]. Thus, the large cations are well immobilized in hollandite tunnels. Hollandite cell symmetry may be tetragonal (I4/m space group) or monoclinic (I2/m space group). This mainly depends on the relative values of the radius of cations in sites A (r_A) and B (r_B) (r_A and r_B are, respectively, the average ionic radii of (Ba,Cs) cations in site A and (M,Ti) cations in site B) [27,28]. Between these two symmetries, the cross-section of the tunnels changes from approximately square in shape (tetragonal cell) to a rhombus shape (monoclinic cell). The trivalent and divalent cations M in site B insured charge compensation of the positive charge excess in the tunnels due to cesium and barium ions. In tetragonal hollandites, all octahedral sites B are identical whereas in monoclinic hollandites two different types of sites B can be distinguished [18]. In this work, it appeared that all hollandite XRD patterns could be indexed in the I4/m space group (tetragonal symmetry). Theoretically, a maximum of two ($Ba^{2+} + Cs^{+}$) cations per unit formula (i.e. $x + y = 2$) can be incorporated in the hollandite structure. However, it is only for small monovalent cations (such as K^{+}) that the box-shaped cavities (site A) in the tunnels of hollandite can be all occupied ($K_2(Al_2Ti_6)O_{16}$) [24]. For hollandites containing only Ba^{2+} ions ($y = 0$) or a mixture of Ba^{2+} and Cs^{+} ions, tunnels are only partially occupied ($x + y < 2$) because vacant sites are necessary to accommodate both repulsion between Ba^{2+} ions and local distortions that occurred after incorporation of big Cs^{+} ions. Moreover, as indicated above, studies performed on various compositions showed that stable hollandite existed only for $x + y > 1$ [13]. Indeed, for each hollandite there is a lower limit of $(x + y)$ below which the intended composition cannot be obtained as a single phase and a fraction of TiO_2 remained as secondary phase in ceramics. For instance, according to Zandbergen et al. [13], $Ba_x(Al,Ti)_8O_{16}$

hollandite can be obtained as a single phase only for $1.16 < x < 1.28$ (Table 2).

Depending on hollandite composition and more particularly on the nature of cations M, vacant sites and cations in the tunnels may take up an ordered arrangement (modulated structure with superlattice ordering) [27,29]. In a recent XRD study of (Ba,Al)- and (Ba,Al + Fe)-hollandite single crystals prepared by flux method, we confirmed the existence of a modulated incommensurate structure: all diffraction spots could be indexed in the superspace group I4/m(00γ)00, where (00γ) are the coordinates of the modulation vector in reciprocal space [23,30]. This incommensurate structure was due to a modulation of barium occupancy level along the tunnels. Concerning cations M in site B, it was shown that their size had a strong effect on the average (M,Ti)–O distance d, the cell volume V and the box-shaped cavities (site A) volume V_c, as d, V and V_c increase with cation M radius [18]. The size of tunnel walls of hollandite is mainly controlled by cations in site B and not by cations in site A. This explains why partial reduction of titanium ions in Synroc-hollandite or partial substitution of Al^{3+} ions by bigger Fe^{3+} ions (Table 1) facilitates cesium incorporation in tunnels and thus avoids the formation of parasitic phases with low chemical durability such as $CsAlTiO_4$ [31,32].

3. Experimental procedures

3.1. Synthesis of hollandite ceramic

(Ba,Cs,M)-hollandite ceramics of formula $(Ba_x^{2+}Cs_y^{+})(M_z^{3+}Ti_{8-z}^{4+})O_{16}$ with $z = 2x + y$ for charge compensation reasons and with for $M^{3+} = Al^{3+}$, Cr^{3+}, Ga^{3+}, Fe^{3+} and Sc^{3+} were prepared by solid-state reaction from reagent-grade oxide, carbonate and nitrate powders (oxide route): Al_2O_3, TiO_2, $BaCO_3$, Cr_2O_3, Fe_2O_3, Ga_2O_3, Sc_2O_3, $CsNO_3$. For compositions without Cs ($y = 0$, (Ba,M)-hollandites), $Ba_{1.16}^{2+}(M_{2.32}^{3+}Ti_{5.68}^{4+})O_{16}$ ceramics were synthesized for each trivalent cation. Whereas, for compositions with Cs ($y \neq 0$, (Ba,Cs,M)-hollandites), $(Ba_{1.04}^{2+}Cs_{0.24}^{+})(M_{2.32}^{3+}Ti_{5.68}^{4+})O_{16}$ ceramics were prepared only for $M^{3+} = Fe^{3+}$, Cr^{3+} and Ga^{3+}. Mixed hollandite samples with and without Cs, containing two kinds of trivalent cations M^{3+}, Al^{3+} and Fe^{3+} ions $(Ba_{1.28}(Al_{1.64}Fe_{0.92}Ti_{5.44})O_{16}$; $(Ba_{1.00}Cs_{0.28})(Al_{1.46}Fe_{0.82}Ti_{5.72})O_{16})$ or Al^{3+} and Ga^{3+} ions $(Ba_{1.28}(Al_{1.64}Ga_{0.92}Ti_{5.44})O_{16}$; $(Ba_{1.00}Cs_{0.28})(Al_{1.46}Ga_{0.82}Ti_{5.72})O_{16})$ were also synthesized. A sample with Mg^{2+} ions in octahedral sites $(Ba_{1.16}(Mg_{1.16}Ti_{6.84})O_{16})$ was prepared using MgO as raw material.

The samples were all prepared using the oxide-route method optimized in [20]. One sample $((Ba_{1.00}Cs_{0.28})(Al_{1.46}Fe_{0.82}Ti_{5.72})O_{16})$ was prepared by alkoxide route to compare its structural and microstructural characteristics with those synthesized by oxide route. For oxide route, dried reagent powders (30 g) were mixed and ground with an agate mortar, pelletized and calcined under air for 4 h at 810 °C to decompose carbonates and nitrates. At this stage hollandite phase was not formed but $BaTi_2O_5$ and $BaTiO_3$ were identified by XRD for the samples with $y = 0$ and $M^{3+} = Al^{3+}$. Once ground again for 1 h with an attrition mill to increase the homogeneity and reactivity of the precursor mixture, calcined powders were pelletized (30 MPa) and sintered at 1200 °C during 30 h in air. Attrition mill contained water and 0.6–0.8 mm diameter zirconia-base silicate glass-ceramic balls. After milling, the particle size of hollandite precursors mixture was smaller than 1 μm. In some cases, in particular for compositions with cesium and gallium or iron, samples were also prepared using attrition balls made of yttrium stabilized zirconia to suppress contamination of powders by silica during milling.

$(Ba_{1.00}Cs_{0.28})(Al_{1.46}Fe_{0.82}Ti_{5.72})O_{16}$ ceramic was also prepared using the alkoxide route described in reference [11]. Titanium isopropoxide and aluminum secbutoxide were dissolved in ethanol. An aqueous solution of Fe, Ba and Cs nitrates was then added to the alkoxides mixture. This mixture was then stir-dried, calcined at 1000 °C (2 h), milled for 1 h with in a planetary ball milling using yttrium stabilized zirconia balls (3 mm diameter) and pelletized (120 MPa) before sintering under air at 1250 °C for 15 h.

3.2. Characterization methods

All ceramic samples were characterized by X-ray diffraction (XRD) with CoK_α wavelength ($\lambda = 1.78897$ Å), scanning electron microscopy (SEM), energy dispersive X-ray analysis (EDX) and in some cases by electron probe microanalysis (EPMA). The following natural or synthetic samples of known compositions were used as standards to determine by EPMA the composition of the major (hollandite) and minor phases of the ceramics: $BaSO_4$ (Ba), $CsTiAsO_5$ (Cs), Al_2O_3 (Al), Fe_2O_3 (Fe), $MnTiO_3$

(Mn), Ga_2O_3 (Ga), $ScPO_4$ (Sc), Cr_2O_3 (Cr), olivine (Mg), $ZrSiO_4$ (Zr), apatite (P), albite (Si) (for each standard sample, the corresponding element analyzed in hollandite ceramics is given in parenthesis). For SEM, EDX and EPMA characterizations, ceramic samples were polished with an anhydrous alcoholic solution to avoid the dissolution of parasitic phases soluble in water that could be present after sintering. The chemical composition of several ceramic samples was also determined by the ICP-AES (Inductively Coupled Plasma-Atomic Emission Spectrometry) method at the Laboratoire Central d'Analyses du CNRS (Vernaison, France). Compositions determined by ICP-AES corresponded to average composition of ceramics (hollandite + parasitic phases) whereas compositions obtained by EPMA corresponded only to the phase probed by the electron beam. Several samples ((Ba,Al)- and (Ba,Fe)-ceramics) were also characterized by high resolution transmission electron microscopy (HRTEM) and selected area electron diffraction (SAD) to study the ordering of Ba^{2+} ions and vacancies in the tunnels. The HRTEM study was carried out on a TOPCON 002B microscope fitted with a small-angle double-tilt stage (±10°) and operating at 200 kV. Specimens were prepared by crushing small quantities of the samples in ethanol (in an agate mortar) and then allowing a drop of the resulting suspension to dry on a perforated carbon film. Thin regions of flakes overhanging a hole in the carbon film were then chosen for observation. Numerical treatment by Fourier transform of some TEM images was performed after digitization of the experimental images with a high-resolution scanner.

^{133}Cs MAS NMR (magic angle spinning nuclear magnetic resonance) spectra were also recorded for samples containing cesium with $M^{3+} = Ga^{3+}$ or $(Al^{3+} + Ga^{3+})$. They were collected on a Bruker Avance 300 (and Avance 500 for $CsAlTiO_4$) Wide Bore (WB) spectrometer operating at 39.283 MHz (65.468 MHz, respectively), using a commercial Bruker 4 mm o.d. MAS probe (mass sample ~100 mg), a spinning frequency of 14 kHz and a recycle delay of 1 s. Longer recycle delays provided identical spectra. It was found that for hollandite phase, spectra acquired at lower field (300 WB) exhibited higher signal to noise ratio, suggesting the presence of a significant contribution of chemical shift anisotropy (proportional to the magnetic field). Up to 65,000 scans were acquired using a spin echo pulse sequence (180-τ-90-τ-Acquisition with τ equal to one rotor period) in order to avoid spectrum distortions due to delayed acquisition (dead-time after the end of pulses) and to ringing signals. Chemical shifts are reported in ppm relative to an external sample of 0.5 M CsCl. For comparison with hollandite ceramics spectra, the spectrum of $CsAlTiO_4$ phase was also recorded. This compound was prepared by solid state reaction from $CsNO_3$, Al_2O_3 and TiO_2 powders: calcination at 810 °C (4 h) and sintering at 1200 °C (30 h). Small amounts of secondary phases (Al_2O_3, TiO_2) were observed coexisting with $CsAlTiO_4$ probably because of cesium evaporation during synthesis. Owing to the high concentrations of paramagnetic species in samples with $M^{3+} = Cr^{3+}$, Fe^{3+} and $(Al^{3+} + Fe^{3+})$, NMR studies were not performed for these ceramics. Indeed, the occurrence of high amounts of species with electronic spin $S \neq 0$ generally leads to a strong broadening and/or a shift of NMR signals, as shown for example in the case of high concentration of paramagnetic Ti^{3+} ions in hollandite [32]. MAS-NMR ^{133}Cs (100% natural abundance, $I = 7/2$) spectra were used to determine the number of different Cs environments in ceramics. Chemical shift gave information about the nature of the phases in which Cs^+ ions were located by comparison with Cs-rich single phase samples ($CsAlTiO_4$) and literature results.

The density d_A of single phase ceramic samples without cesium ($y = 0$) was measured using the Archimedes' principle in toluene solvent. For comparison, theoretical density (d_{th}) was calculated from composition and lattice parameters determined by XRD. The melting point of single phase hollandite samples without cesium was determined by differential thermal analysis (DTA) in Pt crucibles from the onset of endothermic peak occurring at high temperature ($T > 1400$ °C) using 80–125 μm particle size ceramic powders and a heating rate of 10 °C min^{-1}.

4. Results and discussion

4.1. $Ba_{1.16}(M_{2.32}Ti_{5.68})O_{16}$ hollandites ($M^{3+} = Al^{3+}, Cr^{3+}, Ga^{3+}, Fe^{3+}$)

The XRD patterns of (Ba,M)-hollandite $Ba_{1.16}(M_{2.32}Ti_{5.68})O_{16}$ ($M^{3+} = Al^{3+}$, Cr^{3+}, Ga^{3+}, Fe^{3+}) samples are shown in Figs. 2 and 3. According to these patterns, the samples obtained with $M^{3+} = Al^{3+}$, Cr^{3+}, Ga^{3+} and Fe^{3+} were single-phase hollandite. Except the two broad and weak lines due to modulated structure (superlattice lines,

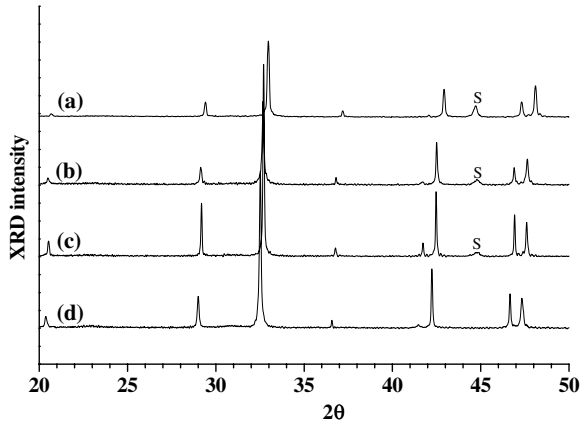

Fig. 2. XRD patterns of (Ba,M)-hollandite $Ba_{1.16}(M_{2.32}Ti_{5.68})O_{16}$($M^{3+} = Al^{3+}$,$Cr^{3+}$,$Ga^{3+}$, Fe^{3+}) samples obtained by oxide route (sintering at 1200 °C). (a) Al^{3+}; (b) Cr^{3+}; (c) Ga^{3+}; (d) Fe^{3+}. All the XRD lines of ceramic samples can be indexed in the I4/m space group of hollandite (tetragonal structure). S: aluminum support (λ $CoK_{\alpha 1} = 1.78897$ Å).

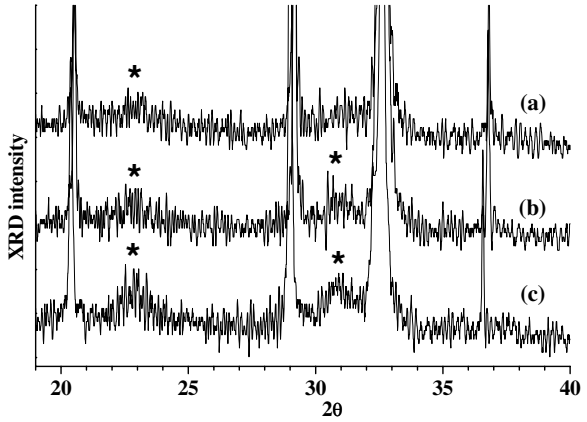

Fig. 3. Extended view of three of the XRD patterns of Fig. 2 ($Ba_{1.16}(M_{2.32}Ti_{5.68})O_{16}$: $M^{3+} = Cr^{3+}$ (a), Ga^{3+} (b), Fe^{3+} (c)) showing superlattice lines, indicated by * (λ $CoK_{\alpha 1} = 1.78897$ Å).

see below) shown in Fig. 3, all XRD lines could be indexed in the I4/m space group (tetragonal structure) and no parasitic phase was detected on the patterns. The corresponding lattice parameters ($a = b$, c) and the cell volume V are given in Table 3. The variation of a and$c$ with the average radius r_B of cations in site B is shown in Fig. 4. It is interesting to notice that literature indicated that the iron (Ba,Fe)-hollandite $Ba_{1.14}(Fe_{2.28}Ti_{5.71})O_{16}$, i.e. a composition very close to the one studied in the present work, was monoclinic ($a = 10.107$ Å, $b = 2.969$ Å, $c = 10.064$ Å, $\beta = 90.077°$) [33]. However, in our case, the lines of the XRD pattern of $Ba_{1.16}Fe_{2.32}Ti_{5.68}O_{16}$ sample (Fig. 2(b)) did not exhibit any splitting as would be expected for a monoclinic structure. This observation was in agreement with more recent results obtained using synchrotron X-ray diffraction for $Ba_xFe_{2x}Ti_{8-2x}O_{16}$ ($1.1 \leqslant x \leqslant 1.3$)-hollandites showing that the structure is tetragonal for $x < 1.2$ [34]. Fig. 4 and Table 3 clearly show that $a = b$,c and V increase with r_B as reported in literature [18,35]. It is easy to understand that the increase of lattice parameters leads to an increase of the size of box-shaped cavities in tunnels (Fig. 1). Consequently, as Al^{3+} ions were the smallest trivalent ions incorporated in site B in this work (Table 1), hollandites with chromium, gallium or iron exhibit larger tunnel cavities than hollandite with aluminum. This expansion of tunnels size is supposed to facilitate Cs incorporation. In Fig. 4 are also reported the lattice parameters of the mixed hollandites with $M^{3+} = (Al^{3+} + Fe^{3+})$ and $M^{3+} = (Al^{3+} + Ga^{3+})$ studied in this work (Table 3). All these data indicate that hollandite lattice parameters increase linearly with r_B. The fact that a parameter increases more strongly with r_B than c parameter (compare the slopes S deduced from linear fits in

Table 3
Lattice parameters of the single-phase Ba-hollandite ceramics prepared in this work

Nominal composition	EPMA composition	a (Å)	c (Å)	V (Å^3)	r_B (Å)	d_A; d_{th}; d_A/d_{th}
$Ba_{1.16}(Al_{2.32}Ti_{5.68})O_{16}$	$Ba_{1.18}(Al_{2.32}Ti_{5.67})O_{16}$	9.968	2.923	290.4	0.584	4.06; 4.29; 0.94
$Ba_{1.16}(Cr_{2.32}Ti_{5.68})O_{16}$	$Ba_{1.16}(Cr_{2.29}Ti_{5.70})O_{16}$	10.054	2.952	298.4	0.608	3.92; 4.49; 0.87
$Ba_{1.16}(Ga_{2.32}Ti_{5.68})O_{16}$	$Ba_{1.18}(Ga_{2.30}Ti_{5.68})O_{16}$	10.051	2.957	298.8	0.609	4.55; 4.72; 0.96
$Ba_{1.16}(Fe_{2.32}Ti_{5.68})O_{16}$	$Ba_{1.13}(Fe_{2.32}Ti_{5.70})O_{16}$	10.103	2.971	303.2	0.616	4.37; 4.47; 0.97
$Ba_{1.28}(Al_{1.64}Fe_{0.92}Ti_{5.44})O_{16}$	$Ba_{1.29}(Al_{1.71}Fe_{0.93}Ti_{5.38})O_{16}$	10.003	2.943	294.5	0.595	nm; 4.44; nm
$Ba_{1.28}(Al_{1.64}Ga_{0.92}Ti_{5.44})O_{16}$	$Ba_{1.29}(Al_{1.65}Ga_{0.85}Ti_{5.48})O_{16}$	9.984	2.938	292.8	0.592	nm; 4.54; nm

$a(= b)$ and c parameters were obtained after refinement of the XRD patterns in the I4/m space group (tetragonal structure). V is the cell volume; d_A is the density deduced from Archimede force and d_{th} is the theoretical density deduced from the lattice parameters and the hollandite composition. The composition of the hollandite obtained by EPMA is also given. r_B is the average radius of the cations in site B calculated from the nominal composition.
nm: not measured.

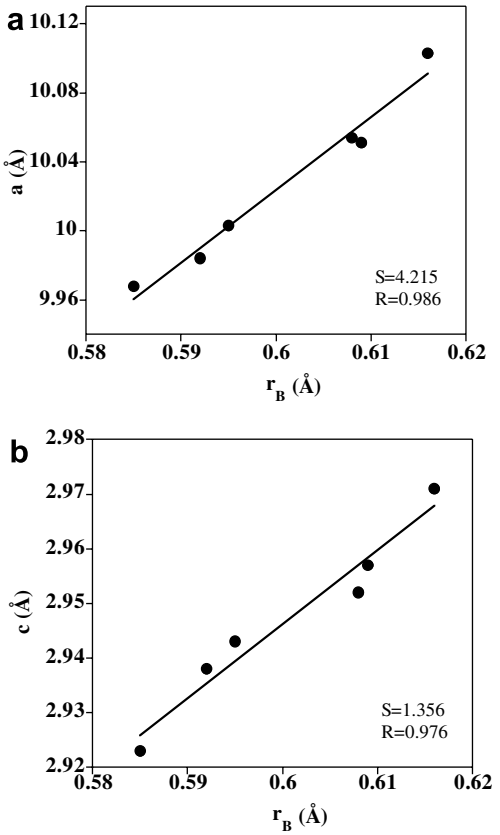

Fig. 4. Evolution of $a(=b)$ and c lattice parameters of single-phase $Ba_{1.16}(M_{2.32}Ti_{5.68})O_{16}$ hollandites ($M^{3+} = Al^{3+}$, Cr^{3+}, Ga^{3+}, Fe^{3+}) prepared in this work versus the average radius $r_B$of cations in site B (see Table 3). The lattice parameters of mixed hollandites with $M^{3+} = (Al^{3+} + Fe^{3+})$ and $M^{3+} = (Al^{3+} + Ga^{3+})$ are also reported in the figure. Least square linear fits of $a(=b)$ and c versus r_B are shown with corresponding slopes (S) and correlation coefficients (R).

Fig. 4) could not be explained easily but agrees with the results of Zhang et al. and Burnham [36]. The evolution of lattice parameters with r_B shows that hollandite structure mainly accommodated the size increase of cations M^{3+} in site B by increasing (Ti,M)–O bond distances perpendicularly to the direction of the tunnels (corresponding to a and b parameters). The slopes S of the linear fits in Fig. 4 are, respectively, equal to 4.21 and 1.35. These values are relatively close to the ones derived by Zhang and Burnham [36] (5.130 and 1.414, respectively, for a and c) and by Fanchon [28] (4.7 and 1.7, respectively, for a and c) from the evolution of the unit-cell parameters with r_B of a high number of hollandite-type phases.

The weak and broad additional lines around 22° and 31° which are observed more clearly on XRD patterns (Fig. 3) for the biggest M^{3+} cations (Ga^{3+}, Fe^{3+}) cannot be indexed in the I4/m space group and correspond to superlattice lines as they occur at positions incommensurate with tetragonal lattice. According to literature [34,37,38], these lines are due to ordered arrangement of Ba^{2+} ions and vacancies in the tunnels. Our XRD study performed on $Ba_{1.16}(Al_{2.32}Ti_{5.68})O_2$ and $Ba_{1.32}(Al_{0.96}Fe_{1.28}Ti_{5.66})O_{16}$ single crystals [23,29] confirmed that these XRD extra-lines are due to the ordering of barium ions and vacancies in the tunnels (modulated structure) and that they can be indexed in I4/m(00γ)00 superspace group. According to several papers [27,39,40], this ordering may extend between adjacent tunnels (lateral correlation) and it was shown to depend on both the size of cations M in site B and on the amount of barium cations in the tunnels (occupancy level). The fact that the width of superlattice lines decreases with increasing the ionic radius of cations M (compare XRD pattern (a) and (c) in Fig. 3) would indicate that the size of ordered domains increases. An explanation of this evolution was proposed by Kesson and White [41] using both structural and electrostatic screening considerations. In agreement with these structural considerations, the present XRD study performed on hollandite single crystals shows that it is more reasonable to consider that the width of superlattice lines is due to the small size of (Ba^{2+}, vacancies) ordered domains rather than to a distribution of modulation vectors [23]. In this case, using Scherrer formula [42] that gives the relation between the size D of ordered domains and the width of XRD lines on patterns, D was estimated to be about 30 Å for (Ba,Ga)- and (Ba,Fe)-hollandites. D would be lower for (Ba,Al)- and (Ba,Cr)-hollandites.

The characterization of $Ba_{1.16}(Al_{2.32}Ti_{5.68})O_{16}$ and $Ba_{1.16}(Fe_{2.32}Ti_{5.68})O_{16}$ ceramics by HRTEM and SAD confirmed that substitution of aluminum by iron ions in site B leads to larger ordered domains. All electron diffraction patterns performed on $Ba_{1.16}(Al_{2.32}Ti_{5.68})O_{16}$ ceramics display diffusion spots and streaks in addition to Bragg spots corresponding to the rutile structure. In Fig. 5(a), the locus of extra-spots aligned along a direction parallel to [001] on each side of every Bragg reflections is directly related to the Ba content. They can be indexed in the I4/m(00γ)00 superspace group with $\gamma = 0.4$. The x value of the Ba content is given by the formula $x = 2(1 - \gamma)$ proposed by Mijhloff

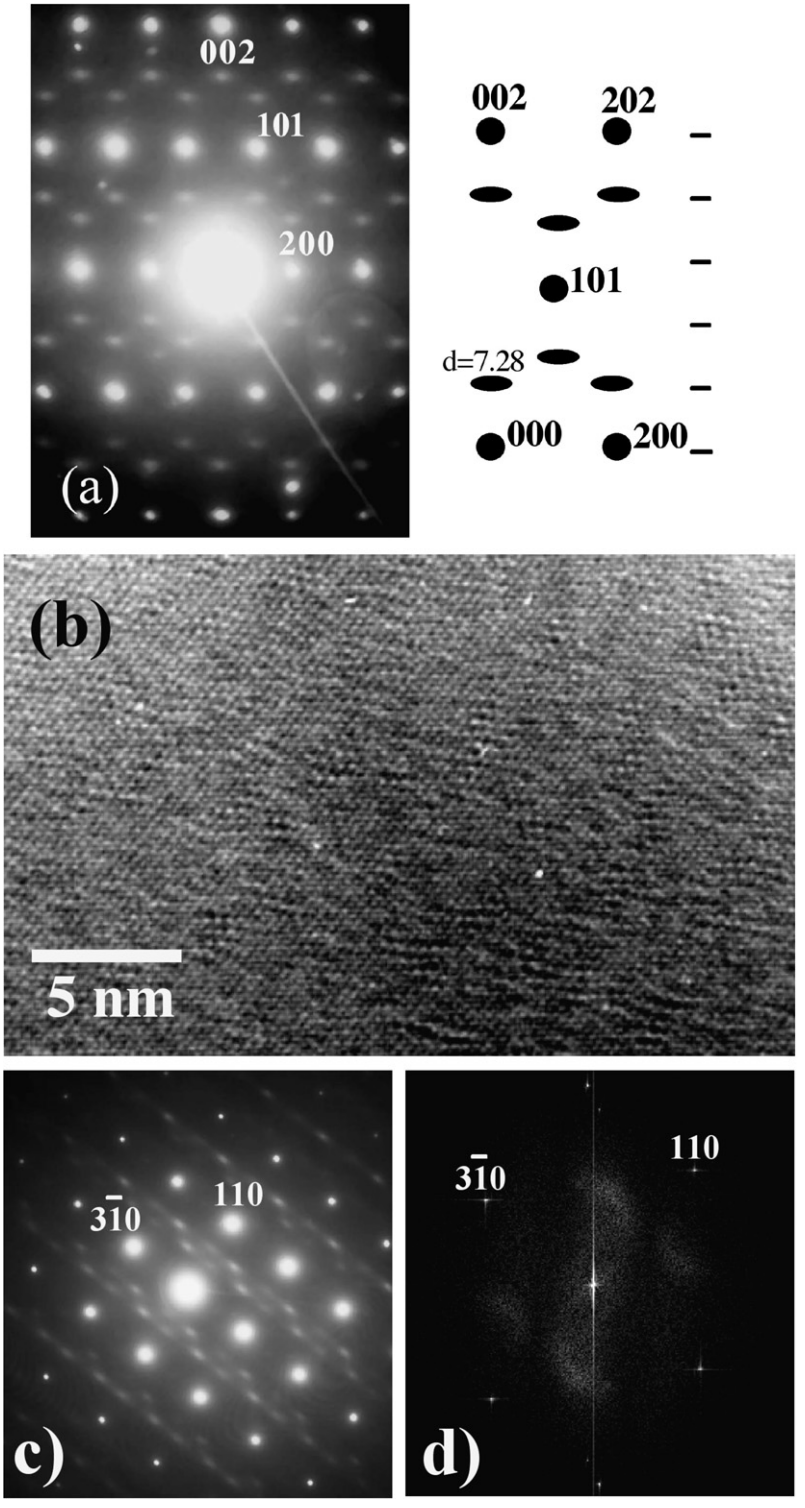

Fig. 5. (a) Electron diffraction pattern (left) and its indexed schematic (right) of the $Ba_{1.16}Al_{2.32}Ti_{5.68}O_{16}$ compound in the [0 1 0] electron beam direction. (b) $Ba_{1.16}Al_{2.32}Ti_{5.68}O_{16}$ hollandite. HRTEM experimental image corresponding to the [1 3 −3] zone axis. (c) Selected area diffraction pattern corresponding to a large zone including the HRTEM image (b). (d) Power spectrum of the digitized HRTEM image (b). (e) Ordered domains revealed by difference between the experimental image (b) and the image reconstructed by Inverse Fourier Transform from Bragg spots 0 1 1 and 3 −1 0 (ideal structure).

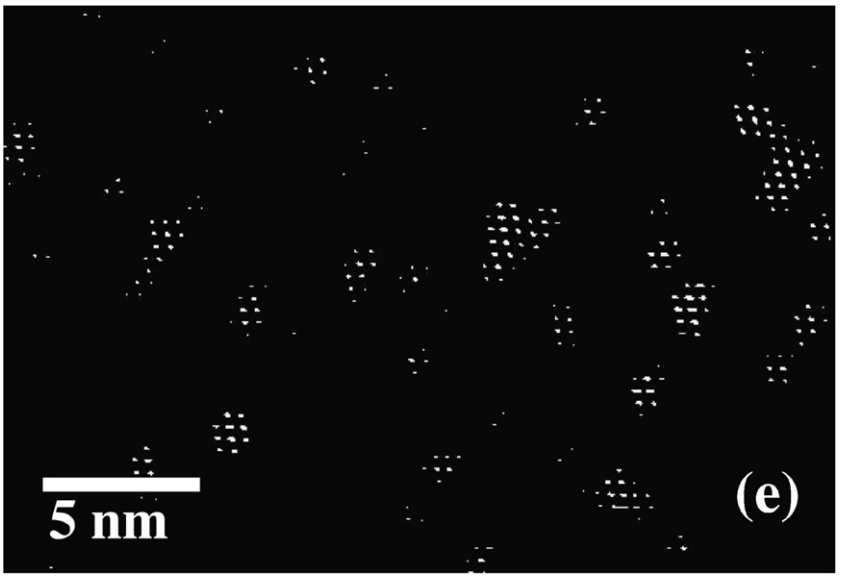

Fig. 5 (*continued*)

et al. [50]. For $\gamma = 0.4$ we obtain $x = 1.2$ in good agreement with the composition of the (Ba,Al)-hollandite analyzed by EPMA ($Ba_{1.18}(Al_{2.32}Ti_{5.67})O_{16}$, $x = 1.18$). The modulation vector q along the 001 direction, equal to the ratio $d_{001}/0.728$ corresponding to $2/5c^*$ is related to the distribution of cations A and vacancies ||, in tunnels along the c-axis with the –[A–A–||–A–||]-series. Ellipsoid-like shape elongated in the plane perpendicular to the c^*-axis of these spots reveals that Ba ions are not only ordered along the 001 direction (1D order) but also in the planes perpendicular to that direction, revealing a correlation between tunnels (3D order). These extra-spots and streaks are also visible in diffraction planes not containing the c^*-axis (Fig. 5(b), zone-axis parallel to $[1\,3\,\bar{3}]$) From the digitized HRTEM image (Fig. 5(c)) corresponding to that orientation, we obtained the calculated diffraction pattern (Fig. 5(d)), by using the modulus of the fast Fourier transform (FFT) of a square zone (20×20 nm). Diffusion features appear between Bragg spots of the structure. Image processing allows taking into account either the Bragg spots or the diffuse scattering in the Fourier transform. The reconstruction of images from inverse Fourier transform (IFT) allows to reveal ordered zones. When the IFT is achieved by using only diffusion streaks, we perfectly visualize small clusters with size ranging from 0.2 to 0.5 nm (Fig. 5(e)). These clusters characterize local short range-order areas between atomic rows projected on the observation plane. Their mean size actually is in good agreement with the size calculated from the line width of extra-lines observed on XRD powder diagrams. Another hollandite ceramics was investigated by SAD substituting all Al^{3+} ions by larger Fe^{3+} ions. No scattering diffusion is observed and well-defined extra spots are perfectly visible along the c^*-axis indicating a likely 3 D ordering between tunnels. This result confirms the evolution of broad extra-lines observed on the XRD patterns.

The SEM micrographs of $Ba_{1.16}(M_{2.32}Ti_{5.68})O_{16}$ ($M^{3+} = Al^{3+}$, Cr^{3+}, Ga^{3+}, Fe^{3+}) samples are shown in Fig. 6. For $M^{3+} = Ga^{3+}$ and Fe^{3+}, a parasitic phase A1 – appearing in white in Fig. 6(c) and (d) – was observed. This phase was not detected on XRD patterns due to its low concentration. Moreover, phase A1 could be amorphous due to the occurrence of Si and O in its composition (EDX results). Indeed, it is known that depending on their compositions, phases containing significant amount of SiO_2 could be amorphous. This phase probably also occurred in samples with aluminum and chromium but could not be observed on SEM images because of their high porosity. EDX spectra (not shown) indicate that phase A1 contains P, Ba, O and Si. It could be assumed that silicon originated at least partly from silicate glass-ceramic attrition balls. Indeed, the use of yttrium-stabilized zirconia attrition balls (that were not available at the beginning of this study) led to a decrease of the proportion of phase A1 on SEM images. Phosphorus is a

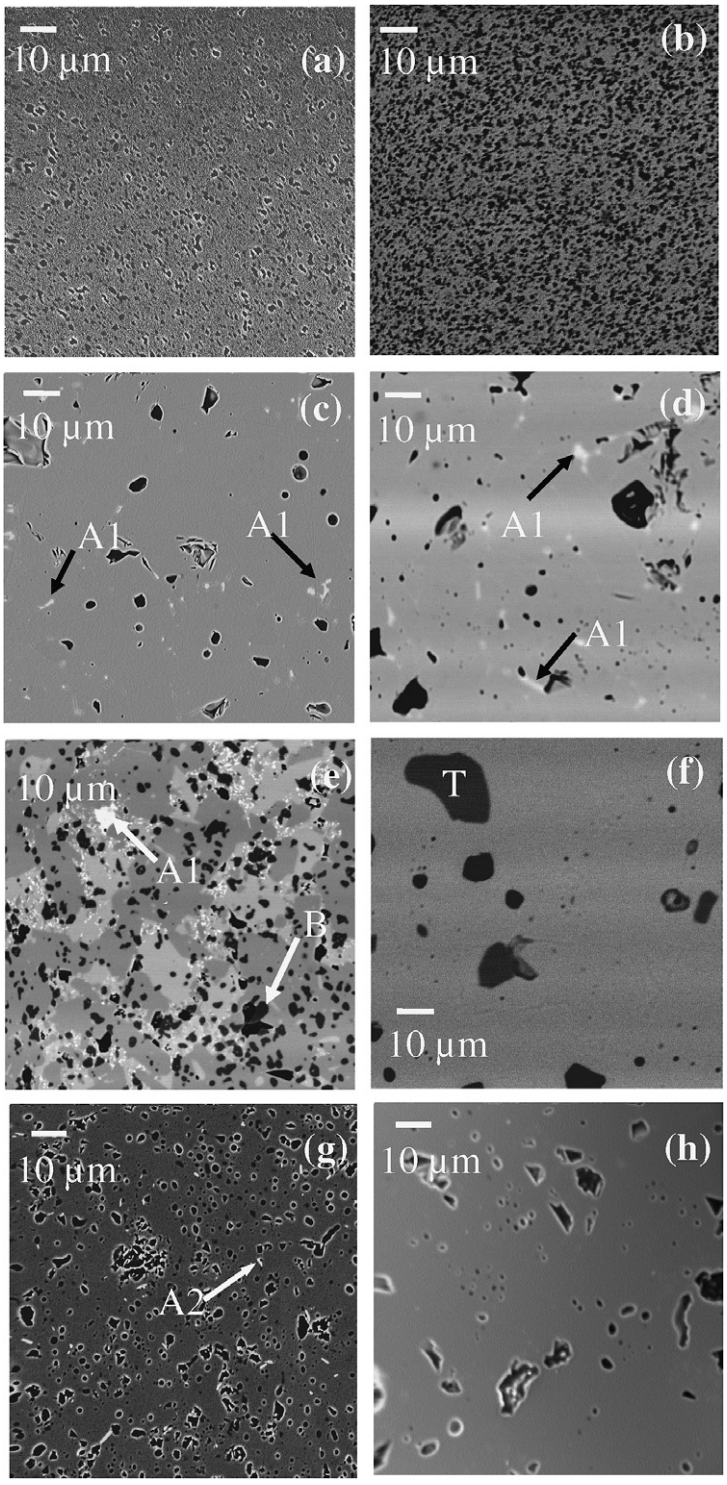

Fig. 6. SEM backscattered electron images of: $Ba_{1.16}(M_{2.32}Ti_{5.68})O_{16}$with M = Al (a), Cr (b), Ga (c), Fe (d), Sc (e); $Ba_{1.16}(Mg_{1.16}Ti_{6.84})O_{16}$ (f) and $Ba_{1.28}(Al_{1.64}Fe_{0.92}Ti_{5.44})O_{16}$ (g). All these samples were prepared following the oxide route (sintering at 1200 °C 30 h). The SEM secondary electrons image of $Ba_{1.16}(Cr_{2.32}Ti_{5.68})O_{16}$ (h) ceramic prepared following the oxide route but with sintering at 1320 °C (30 h) is also shown. The dark regions on (a)–(d), (g) and (h) images correspond to pores. The gray continuous phase observed on all images corresponds to hollandite. T represents TiO_2 (rutile); B represents $Ti_3Sc_4O_{12}$ and A1 represents a parasitic phase containing P, Si, Ba and O; A2 represents a parasitic phase containing Si, Cs and O. Scale bars (10 µm) are indicated in the figures.

common impurity existing in many TiO_2 raw materials. The use of P-free TiO_2 in the mixture before calcination was shown to induce a strong decrease of the quantity of white phase A1 on SEM images. Consequently, in spite of the occurrence of parasitic phase A1 in ceramics for $M^{3+} = Ga^{3+}$ and Fe^{3+}, the samples can be considered as single phase hollandites. The high porosity of $Ba_{1.16}(Al_{2.32}Ti_{5.68})O_{16}$ and $Ba_{1.16}(Cr_{2.32}Ti_{5.68})O_{16}$ samples (Fig. 6(a) and (b)) showed that aluminum and chromium slew down the densification processes of hollandite ceramics. The strongest effect was observed for chromium. The theoretical density d_{th} deduced from lattice parameters and the density d_A measured using Archimedes' principle are given in Table 3. Density values confirmed SEM observations: densification level d_A/d_{th} is the lowest for $M^{3+} = Cr^{3+}$ (13% of porosity). In comparison, (Ba,Fe)- and (Ba,Ga)-hollandites are relatively dense (3% and 4% of porosity, respectively). These results indicate that the chromium-hollandite ceramic obtained after sintering at 1200 °C is not suitable for the application envisaged in this work. Because of its high specific area and porosity such waste form would have low mechanical properties and the access of water would be facilitated in the bulk. Nevertheless, as this ceramic was single phase we tried to incorporate cesium in its structure (see Section 4.3.2). Other studies performed by Leturcq et al. [43] on (Ba,Cr + Al)- and (Ba,Cr + Fe)-mixed hollandite compositions confirmed the negative effect of chromium on the densification of ceramics. The low density of the $Ba_{1.16}(Cr_{2.32}Ti_{5.68})O_{16}$ ceramic prepared at 1200 °C could be explained by the high melting point of both Cr_2O_3 (in comparison with Fe_2O_3, Ga_2O_3 and Al_2O_3 (Table 4)) and chromium-hollandite ($T_M \sim 1650$ °C). Indeed, the melting point determined by DTA for (Ba,Al)-, (Ba,Ga)- and (Ba,Fe)-hollandites (Table 4, Fig. 7) and with the help of an optical pyrometer for (Ba,Cr)-hollandite clearly demonstrated the very high refractory character of $Ba_{1.16}(Cr_{2.32}Ti_{5.68})O_{16}$ hollandite. The same refractory character of Al_2O_3 and $Ba_{1.16}(Al_{2.32}Ti_{5.68})O_{16}$ (Table 4) could also explain the high number of pores observed on the SEM image of $Ba_{1.16}(Al_{2.32}Ti_{5.68})O_{16}$ ceramic (Fig. 6(a)) in comparison with (Ba,Fe)- and (Ba,Ga)-hollandites (Fig. 6(c) and (d)). The effect of the refractory character of both M_2O_3 and $Ba_{1.16}(M_{2.32}Ti_{5.68})O_{16}$ on final ceramic density can be understood by the fact that sintering processes are controlled by atomic diffusion: ions mobility at

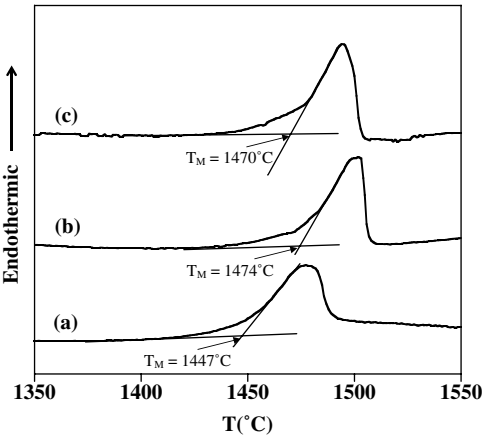

Fig. 7. DTA curves of $Ba_{1.16}(Fe_{2.32}Ti_{5.68})O_{16}$ (a), $Ba_{1.28}(Al_{1.64}Fe_{0.92}Ti_{5.44})O_{16}$ (b) and $(Ba_{1.00}Cs_{0.28})(Al_{1.46}Fe_{0.82}Ti_{5.72})O_{16}$ (c) ceramics showing the endothermic effect associated with melting. The corresponding melting point (Table 4) was determined at the onset of endothermic effect as shown in the figure.

Table 4
Melting point of pure oxides Al_2O_3, Cr_2O_3, Ga_2O_3, Fe_2O_3, Sc_2O_3 and MgO(T_M(Ox)), (Ba,M)-hollandite (T_M(Ba,M-hol)) and (Ba,Cs,M)-hollandite (T_M(Ba,Cs,M-hol)) samples

Cation M	Al^{3+}	Cr^{3+}	Ga^{3+}	Fe^{3+}	Sc^{3+}	$(Al^{3+} + Fe^{3+})$	Mg^{2+}
T_M(Ox) (°C)	2054	2330	1807	1565	2485	nm	2826
T_M(Ba,M-hol) (°C)	1517	1650	1431	1447	nm	1474	nm
T_M(Ba,Cs,M-hol) (°C)	nm	nm	1413	1447	nm	1470	nm

The melting points of pure oxides were taken from Ref. [51]. The composition of the (Ba,M)-hollandite samples were $Ba_{1.16}(M_{2.32}Ti_{5.68})O_{16}$ ($M = Al^{3+}$, Cr^{3+}, Ga^{3+}, Fe^{3+}, Sc^{3+}), $Ba_{1.28}(Al_{1.64}Fe_{0.92}Ti_{5.44})O_{16}$ ($M = Al^{3+} + Fe^{3+}$) and $Ba_{1.16}(Mg_{1.16}Ti_{6.84})O_{16}$ ($M = Mg^{2+}$). The composition of the (Ba,Cs,M)-hollandite samples were $(Ba_{1.04}Cs_{0.24})(Ga_{2.32}Ti_{5.68})O_{16}$ ($M = Ga^{3+}$), $(Ba_{1.04}Cs_{0.24})(Cr_{2.32}Ti_{5.68})O_{16}$ ($M = Cr^{3+}$) and $(Ba_{1.00}Cs_{0.28})(Al_{1.46}Fe_{0.82}Ti_{5.72})O_{16}$ ($M = Fe^{3+}$). The melting point of hollandite samples was determined from the onset of the endothermic effect on DTA curves. The DTA curves of $Ba_{1.16}(Fe_{2.32}Ti_{5.68})O_{16}$, $Ba_{1.28}(Al_{1.64}Fe_{0.92}Ti_{5.44})O_{16}$ and $(Ba_{1.00}Cs_{0.28})(Al_{1.46}Fe_{0.82}Ti_{5.72})O_{16}$ samples are shown in Fig. 7. As the limit of our DTA apparatus was about 1600 °C, the melting point of $Ba_{1.16}(Cr_{2.32}Ti_{5.68})O_{16}$ was estimated with an optical pyrometer.
nm: not measured.

1200 °C is facilitated for the less refractory samples [44]. This leads to difficulties during densification of (Ba,Cr)- and (Ba,Al)-hollandites because of the low sintering temperature (1200 °C) used in this study. However, we showed that the $Ba_{1.16}(Cr_{2.32}Ti_{5.68})O_{16}$ hollandite ceramic can be relatively well densified with sintering at 1320 °C (30 h) (Fig. 6(h)).

The XRD patterns (not shown) and SEM images (Fig. 6(g)) of the mixed hollandite $Ba_{1.28}(Al_{1.64}Ga_{0.92}Ti_{5.44})O_{16}$ and $Ba_{1.28}(Al_{1.64}Fe_{0.92}Ti_{5.44})O_{16}$ ceramics indicated that these samples were single phase. Moreover, as above for ceramics without aluminum, we observed that the occurrence of iron or gallium in hollandite composition led to a decrease of porosity in comparison with $Ba_{1.16}(Al_{2.32}Ti_{5.68})O_{16}$ ceramic. This result confirmed the positive effect of iron and gallium on hollandite densification. It is interesting to notice that the melting point of the mixed $Ba_{1.28}(Al_{1.64}Fe_{0.92}Ti_{5.44})O_{16}$ hollandite (1475 °C) was intermediate between that of $Ba_{1.16}(Fe_{2.32}Ti_{5.68})O_{16}$ (1444 °C) and $Ba_{1.16}(Al_{2.32}Ti_{5.68})O_{16}$ (1517 °C) hollandites. This could explain why the porosity of mixed sample (Fig. 6(g)) was intermediate between the one of samples with only aluminum (Fig. 6(a)) or iron (Fig. 6(d)).

The composition of $Ba_{1.16}(M_{2.32}Ti_{5.68})O_{16}$ ($M^{3+} = Al^{3+}$, Cr^{3+}, Ga^{3+}, Fe^{3+})-hollandites and of mixed hollandites determined by EPMA are given in Table 3. A good agreement was observed between these values and nominal compositions, which is in accordance with the single phase character of all these ceramics.

4.2. $Ba_{1.16}(Sc_{2.32}Ti_{5.68})O_{16}$ and $Ba_{1.16}(Mg_{1.16}Ti_{6.84})O_{16}$ hollandites

The XRD patterns (Fig. 8) and SEM images (Fig. 6(e) and (f)) of $Ba_{1.16}(Sc_{2.32}Ti_{5.68})O_{16}$ and $Ba_{1.16}(Mg_{1.16}Ti_{6.84})O_{16}$ samples clearly show that these ceramics are not single phase.

For (Ba,Mg)-hollandite sample, a high amount of TiO_2 (probably rutile) was observed coexisting with hollandite on SEM images (Fig. 6(f)). As the main XRD lines of rutile are known to occur in the same angular range as the lines of the (Ba,Mg)-hollandite phase, they are probably hidden in Fig. 8(b). Rutile was also observed by Cheary and Squadrito [39] in their (Ba,Mg)-hollandite ceramics outside the single phase $Ba_x(Mg_xTi_{8-x})O_{16}$ domain ($1.14 \leqslant x \leqslant 1.33$). However, as no electron microscopy study was reported in their work, the occurrence of a small amount of TiO_2 could not be totally excluded even for the compositions inside the single phase domain. Both the very high refractory character of MgO (Table 4) and the high radius difference between Ti^{4+} and Mg^{2+} ions (Table 1) in site B could be at the origin of the reactivity difficulties encountered during sintering. The lines splitting observed on XRD pattern of (Ba,Mg)-hollandite ceramic (Fig. 8(b)) indicate that, contrary to the

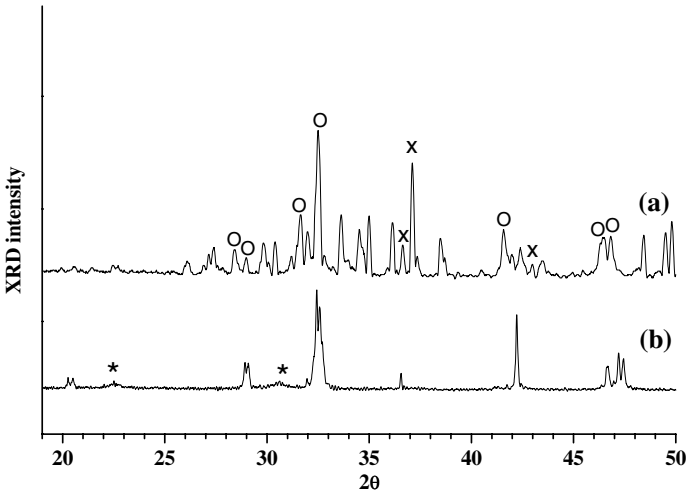

Fig. 8. XRD patterns of $Ba_{1.16}(Sc_{2.32}Ti_{5.68})O_{16}$ (a) and $Ba_{1.16}(Mg_{1.16}Ti_{6.84})O_{16}$ (b) samples prepared by oxide route (sintering at 1200 °C). Pattern (a) clearly shows that $Ba_{1.16}(Sc_{2.32}Ti_{5.68})O_{16}$ ceramic was multiphase: only several lines were attributed (O for hollandite phase, X for $Ti_3Sc_4O_{12}$). All lines of pattern (b) can be indexed in the space group I2/m of monoclinic hollandite, excepted superlattice lines (*). As the main XRD lines of rutile (observed as secondary phase on SEM images, Fig. 6(f)) occurred in the same angular ranges as the ones of (Ba,Mg)-hollandite, they were probably hidden on pattern (b) (λ $CoK_{\alpha 1} = 1$, 78897 Å).

(Ba,Al)-, (Ba,Cr)-, (Ba,Ga)- and (Ba,Fe)-hollandites studied in this work (Fig. 2), the hollandite phase with magnesium has a monoclinic structure (I2/m space group). This structural change, from tetragonal to monoclinic for (Ba,Mg)-hollandite ceramic, could be explained by the high r_B value for this sample (Table 1). In spite of the multiphase character of ceramics with Mg, the composition of hollandite phase determined by EPMA ($Ba_{1.14}(Mg_{1.07}Ti_{6.91})O_{16}$) do not strongly differ from nominal composition.

For (Ba,Sc)-hollandite sample, a high amount of secondary phases coexisting with hollandite phase is detected by XRD and SEM (Figs. 6(e) and 8(a)). Among these phases, $Ti_3Sc_4O_{12}$ is identified unambiguously by XRD but numerous lines are not attributed. The dark phase (Fig. 6(e)) containing only Ti, Sc and O according to EDX, could correspond to $Ti_3Sc_4O_{12}$. The (Ba,P,Si,O)-rich parasitic phase already observed for (Ba,Fe)- and (Ba,Ga)-hollandites is also detected by EDX (white phase A1 in Fig. 6(e)). The contrast variations observed for the continuous phase appearing in grey on SEM images (Fig. 6(e)) could be either due to the unidentified secondary phases or to hollandite composition variations. As no significant evolution of EDX spectra is observed between the grey phases, the second hypothesis seems to be more favorable. In order to avoid the formation of secondary phases, a (Ba,Sc)-hollandite sample was sintered at higher temperature (1320 °C, 30 h) but the ceramics remained multiphase. As $Ba_{1.16}(Sc_{2.32}Ti_{5.68})O_{16}$ composition was slightly outside the single-phase domain reported by Zandbergen et al. ($1.18 \leqslant x \leqslant 1.34$, Table 2), we tried to prepare another composition ($Ba_{1.28}(Sc_{2.56}Ti_{5.44})O_{16}$) inside this domain using the same preparation method (sintering at 1200 °C). Even if the proportion of secondary phases decreases, $Ti_3Sc_4O_{12}$ is still observed in ceramic. As for (Ba,Mg)-hollandite, the strong difficulties to obtain single phase (Ba,Sc)-hollandite at 1200 °C are probably linked to both the very high melting point of Sc_2O_3 (2485 °C) in comparison with all trivalent oxides used in this work (Table 4) and to the high radius difference between Sc^{3+} and Ti^{4+} ions (Table 1). It is interesting to notice that the hollandite radius ratio tolerance factor t_H – that can be calculated from geometrical considerations according to the formula given in the legend of Table 1 [45] – is the lowest for the Sc-hollandite composition ($t_H = 0.966$). According to literature [45], for a given hollandite composition, the value of t_H gives an indication on the stability of the corresponding hollandite structure: the more stable structures correspond to t_H values close to one, i.e. hollandites in which the big cations Ba^{2+} and Cs^+ fit within the tunnels. The relatively low t_H value of the (Ba,Sc)-hollandite indicates that Ba^{2+} ions do not fit very well the tunnels. Consequently, this structure is less stable than that of the other hollandite compositions prepared in this work (Table 1). Probably both the high melting point of Sc_2O_3 (Table 4) and the lowest stability of the (Ba,Sc)-hollandite are responsible for the multi-phase character of the ceramic.

4.3. (Ba,Cs,M)-hollandites ($M^{3+} = Al^{3+}$, Cr^{3+}, Ga^{3+}, Fe^{3+})

As (Ba,Mg)- and (Ba,Sc)-hollandite ceramics were not single phase, we prepared (Ba,Cs,M)-hollandite ($(Ba_{1.04}Cs_{0.24})(M_{2.32}Ti_{5.68})O_{16}$) samples only with $M = Cr^{3+}$, Ga^{3+} and Fe^{3+}, keeping the same preparation method as above (sintering at 1200 °C during 30 h). For $M = Al^{3+}$, we will only recall here the main results concerning a (Ba,Cs,Al)-hollandite composition with a low amount of cesium ($(Ba_{1.11}Cs_{0.10})(Al_{2.32}Ti_{5.68})O_{16}$) and reported in a previous

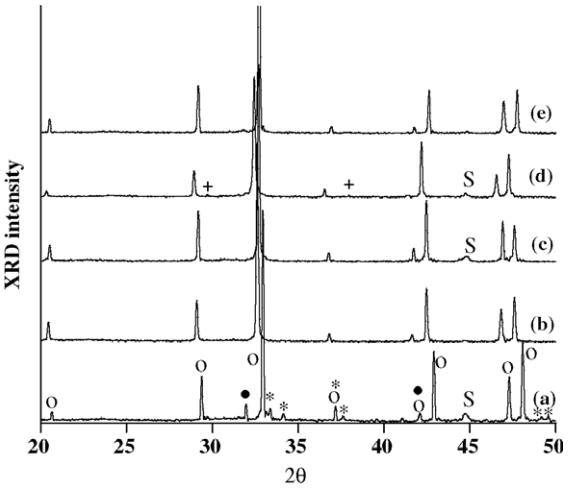

Fig. 9. XRD patterns of (Ba,Cs,M)-hollandite samples prepared following the oxide route (sintering at 1200 °C 30 h). $(Ba_{1.11}Cs_{0.10})(Al_{2.32}Ti_{5.68})O_{16}$ (a); $(Ba_{1.04}Cs_{0.24})(Cr_{2.32}Ti_{5.68}O_{16})$ (b); $(Ba_{1.04}Cs_{0.24})(Ga_{2.32}Ti_{5.68})O_{16}$ (c); $(Ba_{1.04}Cs_{0.24})(Fe_{2.32}Ti_{5.68})O_{16}$ (d); $(Ba_{1.00}Cs_{0.28})(Al_{1.46}Fe_{0.82}Ti_{5.72})O_{16}$ (e). For (Ba,Cs,Al)-ceramic (pattern (a)), the XRD lines corresponding to hollandite (O), TiO_2 rutile (●), $Ba_2Ti_9O_{20}$ (*), Fe_2TiO_5 (+) are shown and aluminum support (S). The main XRD line of $BaTi_4O_9$ which occurs at $2\theta = 35.1°$ is only visible when the XRD pattern of $(Ba_{1.04}Cs_{0.24})(Fe_{2.32}Ti_{5.68})O_{16}$ is zoomed (λ $CoK_{\alpha 1} = 1.78897$ Å).

Table 5
Lattice parameters, composition and parasitic phases of the (Ba,Cs)-hollandite ceramics prepared in this work

Nominal composition	EPMA composition	a (Å)	c (Å)	V (Å^3)	Parasitic phases
$(Ba_{1.11}Cs_{0.10})(Al_{2.32}Ti_{5.68})O_{16}^{i}$	$(Ba_{1.17}Cs_{0.05})(Al_{2.30}Ti_{5.67})O_{16}^{E}$ $(Ba_{1.22}Cs_{0.01})(Al_{2.49}Ti_{5.52})O_{16}^{A}$	9.972	2.923	290.7	TiO_2^e; $Ba_2Ti_9O_{20}^e$
$(Ba_{1.04}Cs_{0.24})(Cr_{2.32}Ti_{5.68})O_{16}^{g}$	$(Ba_{1.08}Cs_{0.11})(Cr_{2.10}Ti_{5.86})O_{16}^{E}$	10.069	2.951	299.3	nd
$(Ba_{1.04}Cs_{0.24})(Cr_{2.32}Ti_{5.68})O_{16}^{h}$	$(Ba_{1.11}Cs_{0.06})(Cr_{2.09}Ti_{5.86})O_{16}^{E}$	nm	nm	nm	nd
$(Ba_{1.04}Cs_{0.24})(Ga_{2.32}Ti_{5.68})O_{16}^{g}$	$(Ba_{1.15}Cs_{0.15})(Ga_{2.45}Ti_{5.55})O_{16}^{E}$	10.065	2.963	300.1	$CsGaSi_{0.4}Ti_{0.6}O_4^f$
$(Ba_{1.00}Cs_{0.28})(Al_{1.46}Ga_{0.82}Ti_{5.72})O_{16}^{i}$	$(Ba_{1.05}Cs_{0.24})(Al_{1.41}Ga_{0.76}Ti_{5.78})O_{16}^{E}$	10.030	2.937	295.5	$Cs(Al_{0.5}Ga_{0.5})TiO_4^f$
$(Ba_{1.04}Cs_{0.24})(Fe_{2.32}Ti_{5.68})O_{16}^{i}$	$(Ba_{1.06}Cs_{0.26})(Fe_{2.28}Ti_{5.70})O_{16}^{E}$ $(Ba_{1.10}Cs_{0.24})(Fe_{2.35}Ti_{5.65})O_{16}^{A}$	10.122	2.972	304.5	$Fe_2TiO_5^e$
$(Ba_{1.04}Cs_{0.24})(Fe_{2.32}Ti_{5.68})O_{16}^{j}$	$(Ba_{0.97}Cs_{0.21})(Fe_{2.23}Ti_{5.79})O_{16}^{E}$	10.118	2.972	304.2	$Fe_2TiO_5^e$; $BaTi_4O_9^e$; phase containing $(Cs,Si,Ti,O)^f$
$(Ba_{1.00}Cs_{0.28})(Al_{1.46}Fe_{0.82}Ti_{5.72})O_{16}^{j}$	$(Ba_{1.05}Cs_{0.25})(Al_{1.43}Fe_{0.98}Ti_{5.74})O_{16}^{E}$ $(Ba_{1.08}Cs_{0.21})(Al_{1.45}Fe_{0.84}Ti_{5.69})O_{16}^{A}$	10.042	2.942	296.7	One phase containing Cs,Si,O^f
$(Ba_{1.00}Cs_{0.28})(Al_{1.46}Fe_{0.82}Ti_{5.72})O_{16}^{k}$	$(Ba_{1.00}Cs_{0.28})(Al_{1.44}Fe_{0.79}Ti_{5.76})O_{16}^{E}$	10.054	2.944	297.6	Three phases containing, respectively, Y,Zr,O^f; Cs,Si,O^f; Al,O^f

a ($= b$) and c parameters were obtained after refinement of the XRD patterns in the I4/m space group (tetragonal structure). V: cell volume. The composition of the hollandite phase was obtained by EPMA (E) and the composition of the ceramic sample (hollandite + parasitic phases) was determined by the ICP-AES method (A). Parasitic phases were detected either by XRD + SEM (e) or only by SEM (f). (g): ceramic sintered at 1200 °C for 30 h; (h): ceramic sintered at 1320 °C for 30 h; (i): ceramic prepared by oxide route (sintering 1200 °C 30 h) and using yttrium stabilized zirconia attrition balls; (j): ceramic prepared by oxide route (sintering 1200 °C 30 h) and using zirconia-based silicate glass-ceramics attrition balls (k): ceramic prepared by alkoxide route and using yttrium stabilized zirconia balls. (l): ceramic sintered at 1200 °C for 96 h.
nd: not detected; nm: not measured.

work [20]. The results concerning the incorporation of cesium in mixed (Ba,Cs,Al + Ga)- and (Ba,Cs, Al + Fe)-hollandites are also presented.

For all these samples, XRD patterns show that the hollandite phase crystallizes in tetragonal structure (Fig. 9) and that its lattice parameters increase with the size of M^{3+} cation (Table 5) in agreement with the evolutions observed for hollandite samples without cesium (Table 3 and Fig. 4). Moreover, our results indicate that incorporation of cesium leads to a decrease of the superlattice lines in comparison with hollandites without cesium (these lines are not visible in Fig. 9). A similar evolution was already observed by Cheary and Kwiatkowska [37] comparing the XRD patterns of (Ba,Al)- and (Ba,Cs,Al)- hollandite samples. This evolution indicates a decrease of the size of the ordered domains (cations + vacancies in tunnels) in (Ba,Cs,M)-hollandites. Due to their big size, cesium ions probably disturb cations and vacancies ordering in tunnels (Table 1).

4.3.1. (Ba,Cs,Al)-hollandite

For $M = Al^{3+}$, $(Ba_{1.04}Cs_{0.24})(Al_{2.32}Ti_{5.68})O_{16}$ ceramic was not prepared because previous results concerning the synthesis of $(Ba_{1.11}Cs_{0.10})(Al_{2.32}Ti_{5.68})O_{16}$ ceramic clearly showed that this compound remained multiphase even after 96 h sintering at 1200 °C [20]. In particular, XRD and SEM reveal the existence of high amounts of secondary phases, such as TiO_2 and $Ba_2Ti_9O_{20}$, coexisting with hollandite (Fig. 9(a), Table 5). Moreover, EPMA of this sample showed that only 0.05 Cs per formula unit enter the hollandite phase, which corresponds only to 50% of what is expected (Table 5). The fact that lattice parameters of $Ba_{1.16}(Al_{2.32}Ti_{5.68})O_{16}$ and $(Ba_{1.11}Cs_{0.10})(Al_{2.32}Ti_{5.68})O_{16}$ ceramics are very similar confirmed EPMA results (Tables 3 and 5). Moreover, chemical analysis of this sample by the ICP-AES method indicates that only 10% of the initial cesium amount is retained in the ceramic after sintering (Table 5). Thus, nearly 90% of all cesium evaporate during ceramic preparation. Consequently, this result shows that insertion of a small amount of cesium (0.1 Cs per formula unit) in (Ba,Al)-hollandite using oxide route at 1200 °C and natural sintering in air is very difficult. This can be explained by the fact that Al^{3+} ions in site B are not big enough (Table 1) to allow the incorporation of high cesium amounts in tunnels. In these conditions, we may think that an important fraction of Cs do not react with other raw materials of the mixture and evaporated during sintering. However, as Fe^{3+} and Ga^{3+} ions are bigger than Al^{3+} ion (Table 1), the mixed $(Ba_{1.00}Cs_{0.28})(Al_{1.46}Fe_{0.82}$-

$Ti_{5.72})O_{16}$ and $(Ba_{1.00}Cs_{0.28})(Al_{1.46}\ Ga_{0.82}Ti_{\ 5.72})O_{16}$ ceramics were prepared to try to incorporate cesium in hollandite tunnels.

4.3.2. (Ba,Cs,Cr)-hollandite

The XRD pattern and SEM image of the $(Ba_{1.04}Cs_{0.24})(Cr_{2.32}Ti_{5.68})O_{16}$ ceramic are given in Figs. 9(b) and 10(a), respectively. XRD pattern is very similar to that of $Ba_{1.16}(Cr_{2.32}Ti_{5.68})O_{16}$ (Fig. 2(d)). Because of its high porosity, it is difficult to appreciate the single phase character by SEM. Also EPMA analysis (Table 5) shows that less than 50% of the expected amount of cesium is incorporated in hollandite. Consequently, a high fraction of cesium either evaporated during sintering or entered a parasitic phase which is no detected by XRD and SEM. Comparison of the lattice parameters of (Ba,Cr)-hollandites with and without Cs shows that incorporation of Cs^+ ions in tunnels leads to a slight increase of $a(=b)$ parameter (Tables 3 and 5) indicating expansion of tunnels section.

To try to improve ceramic densification, a $(Ba_{1.04}Cs_{0.24})(Cr_{2.32}Ti_{5.68})O_{16}$ sample was sintered at higher temperature (1320 °C 30 h). For comparison, a $Ba_{1.16}(Cr_{2.32}Ti_{5.68})O_{16}$ ceramic sample was also prepared in these conditions. The sample with cesium is still characterized by a high porosity (Fig. 10(b)) but less than previously (Fig. 10(a)), and EPMA shows that the amount of cesium incorporated in hollandite is lower than for the synthesis at 1200 °C, probably because of a higher cesium vaporization at 1320 °C (Table 5). Fig. 6(h) shows that $Ba_{1.16}(Cr_{2.32}Ti_{5.68})O_{16}$ ceramic sample is well densified. Consequently, the occurrence of cesium in powders mixture disturbs densification of the ceramic because of evaporation phenomena during sintering. The very high porosity of the $(Ba_{1.04}Cs_{0.24})(Cr_{2.32}Ti_{5.68})O_{16}$ sample prepared at 1200 °C (Fig. 10(a)) is probably also due to the strong refractory character of Cr_2O_3 and (Ba,Cs,Cr)-hollandite, as it was the case for $Ba_{1.16}(Cr_{2.32}Ti_{5.68})O_{16}$ (Table 4). All these results show that (Ba,Cr)-hollandite can not be selected for Cs immobilization. Indeed, more than 54% of cesium do not enter the tunnels (for sintering at 1200 °C), and porosity is too high to insure good mechanical properties and chemical durability.

4.3.3. (Ba,Cs,Ga)-hollandite

The XRD pattern and SEM image of the $(Ba_{1.04}Cs_{0.24})(Ga_{2.32}Ti_{5.68})O_{16}$ ceramic are given in Figs. 9(c) and 10(c), respectively. According to XRD, the ceramic appears as single phase but a parasitic phase is detected on SEM images (white phase C in Fig. 10(c)). EDX indicates that phase C contains mainly Cs, Si, Ga, Ti and O. Its composition $CsGaSi_{0.4}Ti_{0.6}O_4$ was determined by EPMA. The similitude between this composition and that of water-soluble $CsAlTiO_4$ could indicate that phase C also exhibits a low chemical durability against water. We have no information about the structure of this phase, however by analogy with the structure of $CsAlTiO_4$ [46], Ga^{3+}, Ti^{4+} and Si^{4+} ions may be all located in tetrahedral sites. It is also interesting to notice that the secondary phase $CsGaTiO_4$, whose composition was similar to that of phase C but in which Si^{4+} ions partly replaced Ti^{4+} ions, was detected by Carter et al. in a (Ba,Cs,Ga)-hollandite ceramic prepared by melting [47].

Concerning the hollandite phase in $(Ba_{1.04}Cs_{0.24})(Ga_{2.32}Ti_{5.68})O_{16}$ ceramic, back-scattered SEM images (Fig. 10(c)) show contrast variations corresponding probably to slight composition variations through the sample. However, EDX and EPMA do not indicate significant variations of composition between areas with different contrasts, and hollandite composition determined by EPMA is $(Ba_{1.15}Cs_{0.15})(Ga_{2.45}Ti_{5.55})O_{16}$ (Table 5). Thus, the amount of cesium incorporated in (Ba,Cs,Ga)-hollandite (0.15 Cs per formula unit) is higher than in (Ba,Cs,Cr)-hollandite (0.05 Cs per formula unit). This composition difference could explain why c parameter increases slightly between (Ba,Ga)- and (Ba,Ga,Cs)-hollandites whereas it remains the same for (Ba,Cr)- and (Ba,Cr,Cs)-hollandites (Tables 3 and 5). Comparison of Figs. 6(c) and 10(c) shows that cesium induces an increase of the ceramic porosity. This difference could be due to cesium evaporation during sintering.

The mixed $(Ba_{1.00}Cs_{0.28})(Al_{1.46}Ga_{0.82}Ti_{5.72})O_{16}$ composition was prepared using yttrium-stabilized zirconia attrition balls. No parasitic phase was detected by XRD, but a phase containing Cs, Al, Ga, Ti and O was observed by SEM (not in the chosen zone shown in Fig. 10(d)). The composition of this phase $Cs(Al_{0.5}Ga_{0.5})TiO_4$ was determined by EPMA. As above, by analogy with $CsAlTiO_4$, this phase probably exhibits low chemical durability. By comparison with $CsGaSi_{0.4}Ti_{0.6}O_4$, Si^{4+} ions are here totally replaced by Ti^{4+} and Ga^{3+} ions are partially replaced by Al^{3+} ions. Thus, both suppression of silicon pollution by changing the nature of attrition balls, and partial replacement of Ga_2O_3 by Al_2O_3 in ceramic composition do not suppress

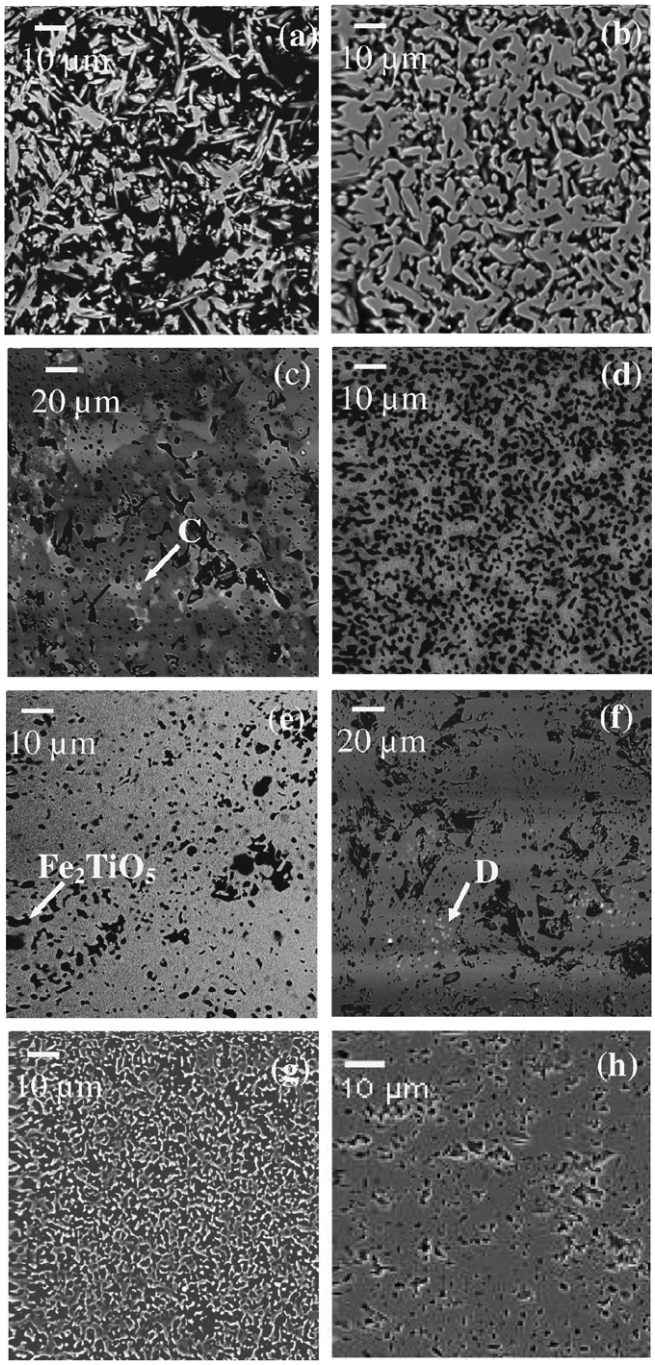

Fig. 10. SEM images of (Ba,Cs,M)-hollandite ceramics: $(Ba_{1.04}Cs_{0.24})(Cr_{2.32}Ti_{5.68})O_{16}$ (a,b); $(Ba_{1.04}Cs_{0.24})(Ga_{2.32}Ti_{5.68})O_{16}$ (c), $(Ba_{1.00}Cs_{0.28})(Al_{1.46}Ga_{0.82}Ti_{5.72})O_{16}$ (d), $(Ba_{1.04}Cs_{0.24})(Fe_{2.32}Ti_{5.68})O_{16}$ (e,f); $(Ba_{1.00}Cs_{0.28})(Al_{1.46}Fe_{2.32}Ti_{5.72})O_{16}$ (g,h). Samples (a,c–g) were prepared following the oxide route with sintering at 1200 °C (30 h). Sample (b) was prepared following the oxide route with sintering at 1320 °C (30 h). Sample (h) was prepared following the alkoxide route (calcination 1000 °C + sintering 1250 °C). (e) and (f) samples were prepared using, respectively, yttrium stabilized zirconia and zirconia base silicate glass-ceramic attrition balls. All the dark regions observed on (a–d,g–h) images correspond to pores. The continuous gray phase observed on all images corresponds to hollandite. C: $CsGaSi_{0.4}Ti_{0.6}O_4$; D: parasitic phase containing Cs, Ti, Si and O. (a–g) back-scattered electrons images. (h) secondary electrons image. Scale bars (10 or 20 µm) are indicated in the figures.

the formation of a Cs-rich parasitic phase, but a decrease of its concentration is always observed. This was confirmed by ^{133}Cs MAS NMR (see below). The decrease of the amount of Cs-rich parasitic phase between (Ba,Cs,Ga)- and (Ba,Cs,Al + Ga)-hollandite samples is in agreement with the increase of cesium concentration in the (Ba,Cs,Al + Ga)-hollandite phase as shown by EPMA ($Ba_{1.05}Cs_{0.24}(Al_{1.41}Ga_{0.76}Ti_{5.78})O_{16}$). Nevertheless, the porosity of the mixed (Ba,Cs,Al + Ga)-hollandite (Fig. 10(d)) is higher than that of (Ba,Cs,Ga)-hollandite (Fig. 10(c)). This observation confirms the negative effect of aluminum on hollandite densification already observed for ceramics without cesium.

The occurrence of a Cs-rich parasitic phase in (Ba,Cs,Ga)-hollandite ceramic is confirmed by ^{133}Cs MAS-NMR. This technique can be used to study hollandite ceramics with gallium because of the low amount of paramagnetic species in these samples contrary to (Ba,Cs,Cr)- and (Ba,Cs,Fe)-hollandites. ^{133}Cs MAS-NMR spectra of $(Ba_{1.04}Cs_{0.24})(Ga_{2.32}Ti_{5.68})O_{16}$ and $(Ba_{1.00}Cs_{0.28})(Al_{1.46}Ga_{0.82}Ti_{5.72})O_{16}$ ceramics and of $CsAlTiO_4$ prepared following the method described in the experimental part are given in Fig. 11. A peak at about 250 ppm is observed for both (Ba,Cs,Ga)- and (Ba,Cs,Al + Ga)-hollandites. The similitude between the two spectra near 250 ppm indicates that the local environment of cesium ions in (Ba,Cs,Al + Ga)-hollandite is very close to that in (Ba,Cs,Ga)-hollandite. A peak occurring in the same chemical shift region was also detected by Carter et al. [19] and Whittle et al. [48] for (Ba,Cs,Al)-hollandite samples. This confirms the incorporation of cesium in the structure of hollandites with gallium. For the (Ba,Cs,Ga)-hollandite sample, an additional broad resonance centered at the peak position of ^{133}Cs in $CsAlTiO_4$ (~41 ppm) is also observed (Fig. 11(b)) and indicates the existence of a secondary phase with cesium in this sample. The position of this line, close to that of cesium in $CsAlTiO_4$ (Fig. 11(a)), is consistent with the $CsGaSi_{0.4}Ti_{0.6}O_4$ phase determined by SEM and EPMA. For the (Ba,Cs,Ga)-sample, no NMR signal is detected near 40 ppm (Fig. 11(c)). This observation agrees with the decrease of the Cs-rich parasitic phase in this sample.

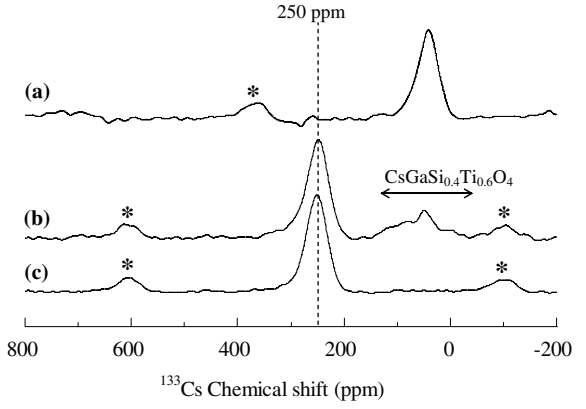

Fig. 11. ^{133}Cs MAS-NMR spectra of $(Ba_{1.04}Cs_{0.24})(Ga_{2.32}Ti_{5.68})O_{16}$ (b) and $(Ba_{1.00}Cs_{0.28})(Al_{1.46}Ga_{0.82}Ti_{5.72})O_{16}$ (c) ceramics prepared using the oxide route. For comparison, the spectrum of the $CsAlTiO_4$ phase is also shown in the figure (a). Spinning sidebands are represented by *. For $(Ba_{1.04}Cs_{0.24})(Ga_{2.32}Ti_{5.68})O_{16}$, an additional broad band attributed to cesium in $CsGaSi_{0.4}Ti_{0.6}O_4$ parasitic phase is indicated. The position of this band is close to that of cesium in $CsAlTiO_4$.

4.3.4. (Ba,Cs,Fe)-hollandite

Two $(Ba_{1.04}Cs_{0.24})(Fe_{2.32}Ti_{5.68})O_{16}$ samples were prepared using either zirconia-base silicate glass-ceramic or yttrium stabilized zirconia attrition balls. The XRD pattern and SEM image of the ceramics obtained after sintering at 1200 °C are given in Figs. 9(d) and 10(e) and (f), respectively. According to XRD and SEM, Fe_2TiO_5, $BaTi_4O_9$ and a Cs-rich phase containing Ti, Si and O are detected as parasitic phases coexisting with hollandite (tetragonal structure) for the sample prepared with zirconia-base silicate glass-ceramic attrition balls. This silicon pollution is suppressed and the parasitic Cs-rich phase is not detected for the sample prepared with yttrium stabilized zirconia attrition balls. Concerning the other parasitic phases, $BaTi_4O_9$ is not detected and the amount of Fe_2TiO_5 decreases for the sample milled with yttrium stabilized zirconia attrition balls. The composition of hollandite phase ($(Ba_{1.06}Cs_{0.26})(Fe_{2.28}Ti_{5.70})O_{16}$, EPMA) and of ceramic sample ($(Ba_{1.10}Cs_{0.24})(Fe_{2.35}Ti_{5.65})O_{16}$, ICP-AES chemical analysis) show that cesium is totally retained in hollandite after synthesis and that iron concentration in the hollandite phase is only slightly lower than in the ceramics. This result confirms the low amount of Fe_2TiO_5 observed for the sample prepared with yttrium stabilized zirconia attrition balls. As Fe_2TiO_5 do not incorporate Cs, the occurrence of this phase is not a serious problem for the use of (Ba,Cs,Fe)-hollandite ceramic as cesium waste form. Moreover, comparison of Figs. 6(d) and 10(e) and (f) shows that cesium incorporation in (Ba,Fe)-hollandite has no significant effect

on ceramic porosity. All these results show that the use of oxide route with sintering at 1200 °C, leads to dense (Ba,Cs,Fe)-hollandite ceramic that can be envisaged to immobilize radioactive Cs. Comparison of (Ba,Fe)- and (Ba,Cs,Fe)-hollandite lattice parameters (Tables 3 and 5) shows that after Cs incorporation in tunnels, the lattice parameter $a(=b)$ increases from 10.103 to 10.122 Å (lateral deformation of the structure, Fig. 1) whereas c remains almost constant, indicating a lack of significant deformation along the tunnels. The increase of $a(=b)$ could be explained both by the increase of the number of cations in tunnels from 1.16 Ba^{2+} ions to 1.28 ($Ba^{2+} + Cs^{+}$) ions per formula unit, and by the increase of the average radius r_A of these cations (from 1.42 to 1.48 Å). The lack of evolution of c parameter is probably due to the vacancies adjacent to Cs^{+} ions in tunnels (0.72 vacancy per formula unit) that compensate the increase of r_A [24].

The mixed $(Ba_{1.00}Cs_{0.28})(Al_{1.46}Fe_{0.82}Ti_{5.72})O_{16}$ ceramic was prepared using both the oxide and alkoxide routes. For the sample prepared by the oxide route with zirconia-based silicate glass-ceramic attrition balls, no parasitic phase is detected by XRD (Fig. 9(e)). Only a very small amount of a parasitic phase containing Cs, Si and O is detected by SEM (Table 5). The Fe_2TiO_5 phase formed in (Ba,Cs,Fe)-hollandite is not observed in the mixed sample. However, due to the high porosity of $(Ba_{1.00}Cs_{0.28})(Al_{1.46}Fe_{0.82}Ti_{5.72})O_{16}$ ceramic (Fig. 10(g)) in comparison with $(Ba_{1.04}Cs_{0.24})(Fe_{2.32}Ti_{5.68})O_{16}$ ceramic (Fig. 10(f)), if parasitic phases exist in mixed ceramic, they are difficult to detect by SEM. As for samples containing gallium, the difference of porosity between these two samples confirms once again the negative effect of aluminum on hollandite densification. Moreover, comparison of Figs. 10(g) and 6(g) demonstrates that cesium disturbs ceramic densification even in the absence of significant vaporization during sintering (see below EPMA and ICP-AES results). This effect could be explained by the large size of Cs^{+} ions (1.74 Å) compared to all the other ions (cations + anions: $r \leqslant 1.44$ Å, Table 1) in our samples. Cesium ions could thus disturb and slew down diffusion processes and porosity elimination during heat treatments. The lattice parameters of hollandite phase (Table 5) show that partial substitution of Fe^{3+} ions by Al^{3+} ions induces a contraction of the cell volume in agreement with radii difference between these ions (Table 1). The composition of hollandite phase ($(Ba_{1.05}Cs_{0.25})(Al_{1.43}Fe_{0.98}Ti_{5.74})O_{16}$, EPMA) and of ceramic sample ($(Ba_{1.08}Cs_{0.21})(Al_{1.45}Fe_{0.84}Ti_{5.69})O_{16}$, ICP-AES) shows that almost all cesium is incorporated in the tunnels of hollandite structure after sintering. The small difference between these compositions could indicate only very low cesium vaporization during synthesis. As for $(Ba_{1.04}Cs_{0.24})(Fe_{2.32}Ti_{5.68})O_{16}$ ceramic, the lack of Cs-rich parasitic phase and of significant cesium vaporization during preparation of $(Ba_{1.00}Cs_{0.28})(Al_{1.46}Fe_{0.82}Ti_{5.72})O_{16}$ sample confirm that total or partial substitution of aluminum by iron in site B facilitates cesium incorporation in site A.

The XRD pattern (not shown) of $(Ba_{1.00}Cs_{0.28})(Al_{1.46}Fe_{0.82}Ti_{5.72})O_{16}$ ceramic prepared by alkoxide route indicates that this sample is single phase. However, study of this ceramic by SEM and EDX shows the existence of three parasitic phases (Table 5): a phase containing Y, Zr and O due to pollution by yttrium stabilized zirconia attrition balls; a phase containing Cs, Si and O probably due to pollution during synthesis and a phase containing mainly Al and O which is probably alumina. As concentration of these parasitic phases is very small and is mainly due to pollution problems during preparation that could be avoided, the ceramic sample prepared by alkoxide route could be considered as single phase. In this sample, the composition of hollandite phase determined by EPMA ($(Ba_{1.00}Cs_{0.28})(Al_{1.44}Fe_{0.79}Ti_{5.76})O_{16}$) shows that cesium is totally retained in tunnels after sintering. It could be underlined that cesium concentration in hollandite phase is only slightly higher for this sample (0.28 Cs per formula unit) than for the sample prepared by oxide route (0.25 Cs per formula unit). This small difference is probably due to slight cesium vaporization during synthesis by oxide route. Comparison of lattice parameters for these two samples (Table 5) indicates that $a(=b)$ increases from 10.042 Å (oxide route) to 10.054 Å (alkoxide route) in agreement with the small increase of Cs concentration in tunnels for the sample prepared by alkoxide route. Moreover, SEM images (Fig. 10(g) and (h)) show that porosity is lower for the ceramic prepared by alkoxide route. Consequently, the use of oxide route to prepare mixed (Ba,Cs,Al + Fe)-hollandite would probably lead to a ceramic with lower mechanical properties and chemical durability. The microstructural differences observed between the two samples could be due to the higher calcination and sintering temperatures (1000 °C and 1250 °C, respectively) used for the alk-

oxide route. XRD shows (pattern not shown) that hollandite phase was already formed in the sample calcined at 1000 °C (alkoxide route) whereas hollandite was only formed after sintering for the sample prepared by the oxide route (calcination at 810 °C). After calcination, Cs^+ ions are thus not incorporated in the tunnels of hollandite for the sample prepared by oxide route and a small fraction of cesium probably evaporates during the sintering stage at 1200 °C. Another $(Ba_{1.00}Cs_{0.28})(Al_{1.46}Fe_{0.82}Ti_{5.72})O_{16}$ ceramic sample was synthesized using the alkoxide route but changing calcination (750 °C 2 h) and sintering (1200 °C 30 h) conditions. In this case, an increase of ceramic porosity and a strong decrease of Cs concentration in the hollandite phase are observed by SEM and EPMA ($(Ba_{1.00}Cs_{0.18})(Al_{1.42}Fe_{0.72}Ti_{5.90})O_{16}$). XRD shows that for this sample the hollandite phase was not formed after calcination. The difference of composition between this sample and that calcined at 1000 °C could also be explained by cesium evaporation during sintering. Consequently, this result tends to confirm the hypothesis proposed above to explain the slight composition differences between samples prepared by oxide or alkoxide routes. To complete this work, it would be interesting to prepare the $(Ba_{1.00}Cs_{0.28})(Al_{1.46}Fe_{0.82}Ti_{5.72})O_{16}$ ceramic by oxide route with a calcination stage at 1000 °C, and to study ceramic microstructure and the amount of Cs incorporated in hollandite structure.

Even if microstructure and composition of the (Ba,Cs,Al + Fe)-hollandite prepared by alkoxide route seemed to indicate that this method is better for Cs immobilization, the results reported above concerning the preparation of the (Ba,Cs,Fe)-hollandite by oxide route clearly demonstrate that a dense ceramic incorporating all cesium can be prepared easily. Thus, total replacement of Al by Fe in hollandite composition allows us to prepare ceramic waste forms adapted to Cs immobilization by oxide route at relative low sintering temperature (1200 °C). This method can thus be considered as an alternative to the alkoxide method largely developed in literature for the preparation of hollandite waste forms.

5. Conclusions

A mixed (Ba,Cs,Al + Fe)-hollandite ($(Ba_{1.00}Cs_{0.28})(Al_{1.46}Fe_{0.82}Ti_{5.72})O_{16}$) was previously proposed by Bart et al. [11] as waste form for Cs immobilization because of its ability to retain all cesium during preparation processes and also because, its low porosity and its high chemical durability. The occurrence of Fe^{3+} ions (coexisting with Al^{3+} ions) in site B of hollandite structure facilitated Cs incorporation in tunnels. In their case, a preparation method using alkoxide and nitrate precursors (alkoxide route) in solution was used to prepare precursor before calcination at 1000 °C and sintering in air at 1250 °C.

In this work, an alternative method (oxide route) was proposed to prepare hollandite waste forms using oxide, carbonate and nitrate powders and classical ceramic processes (grinding + attrition milling + cold pressing + sintering in air). In order to reduce the risks of cesium vaporization during thermal treatments, the sintering temperature was relatively low (1200 °C). Using this method, various ceramic samples have been prepared with and without cesium (corresponding, respectively to $(Ba_{1.04}Cs_{0.24})(M_{2.32}Ti_{5.68})O_{16}$ and $Ba_{1.16}(M_{2.32}Ti_{5.68})O_{16}$ compositions) increasing the size of trivalent M^{3+} cations (Al^{3+}, Cr^{3+}, Ga^{3+}, Fe^{3+}, Sc^{3+}). Using the same synthesis conditions, $Ba_{1.16}(Mg_{1.16}Ti_{6.84})O_{16}$ and mixed (Ba,Al + Fe)- and (Ba,Al + Ga)-hollandites with and without cesium were also prepared. From the microstructural, structural and analytical characterizations of these hollandite ceramics, the following conclusions can be drawn:

(i) For $M^{3+} = Al^{3+}$, Cr^{3+}, Ga^{3+} and Fe^{3+}, a single phase $Ba_{1.16}(M_{2.32}Ti_{5.68})O_{16}$ hollandite ceramics with tetragonal structure was obtained. Mixed hollandite $Ba_{1.28}(Al_{1.64}Ga_{0.92}\ Ti_{5.44})O_{16}$ and $Ba_{1.28}(Al_{1.64}Fe_{0.92}Ti_{5.44})O_{16}$ ceramics were also single phase with tetragonal structure. Only a small amount of parasitic phase containing P, Ba, Si and O was detected by SEM for several samples. This phase originated from impurities in raw materials (P) and contamination by attrition balls during milling (Si). It could be suppressed by changing the purity of raw materials and the nature of attrition balls. Contrary to hollandite with $M = Fe^{3+}$ and Ga^{3+}, hollandite with $M = Al^{3+}$ and Cr^{3+} were low densified after sintering at 1200 °C. This difference was explained by the high melting point of corresponding oxides (Al_2O_3, Cr_2O_3) and hollandites ($Ba_{1.16}(Al_{2.32}Ti_{5.68})O_{16}$, $Ba_{1.16}(Cr_{2.32}Ti_{5.68})O_{16}$) (Table 4). Consequently, the occurrence of aluminum or chromium in hollandite composition slew down densification processes. The strongest effect was observed

with chromium. For mixed (Ba,Al + Fe)- and (Ba,Al + Ga)-hollandites ($Ba_{1.28}(Al_{1.64}Fe_{0.92}Ti_{5.44})O_{16}$ and $Ba_{1.28}(Al_{1.64}Ga_{0.92}Ti_{5.44})O_{16}$), introduction of iron and gallium induced a decrease of ceramics porosity in comparison with $Ba_{1.16}(Al_{2.32}Ti_{5.68})O_{16}$. This confirmed the positive effect of Fe_2O_3 and Ga_2O_3 on densification. Lattice parameters $a(=b)$ and c increased linearly with the average radius r_B of cations in site B. The size of box-shaped cavities (site A) in tunnels increased with r_B. TEM studies performed on the $Ba_{1.16}(Al_{2.32}Ti_{5.68})O_{16}$ composition have confirmed the ordering of Ba^{2+} cations in the tunnels of the hollandite structure by revealing diffusion spots along the c^*-axis on the electron diffraction patterns. The position of these spots was correctly indexed by using the modulation vector determined from X-ray diffraction patterns performed on single crystals with the same composition. Shape of diffusion spots indicates that this ordering is not only 1 D (arrangement of cations and vacancies in the tunnels). Small ordered regions corresponding to a short range order between tunnels were revealed by HRTEM. Their size (2–5 nm) is in good agreement with the mean size of ordered domains determined from the width of broad extra-lines observed on X-ray powder diffraction patterns. For the biggest M^{3+} cations (Ga^{3+}, Fe^{3+}), XRD superlattice lines due to ordered arrangement of Ba^{2+} ions and vacancies in tunnels were observed on patterns in agreement with literature. The HRTEM study actually showed that increasing r_B led to larger ordered domains giving rise to extra-spots instead of scattering diffusion on the electron diffraction patterns.

(ii) $Ba_{1.16}(Sc_{2.32}Ti_{5.68})O_{16}$ and $Ba_{1.16}(Mg_{1.16}Ti_{6.84})O_{16}$ samples prepared at 1200 °C were not single phase. This was probably due to both the high refractory character of MgO and Sc_2O_3 (Table 4) and the high radius difference between Ti^{4+} and (Mg^{2+}, Sc^{3+}) ions in site B (Table 1). This would decrease the reactivity and the ionic diffusion during sintering at 1200 °C. Considerations about hollandite structure stability could also explain the difficulty to obtain single phase (Ba,Sc)-hollandite.

(iii) For $M^{3+} = Al^{3+}$, Cr^{3+} and Ga^{3+}, (Ba,Cs,M)-hollandite ceramics were shown to retain only a fraction of Cs in their structure and were either multi phase and/or poorly densified after sintering at 1200 °C. Both the refractory character of Cr_2O_3 and (Ba,Cr)-hollandite (Table 4) and the small size of Al^{3+} ions (Table 1) could explain the strong difficulties of Cs^+ ions to enter the (Ba,Al)- and (Ba,Cr)-hollandite tunnels. In this case, a high fraction of cesium vaporized during synthesis and disturbed densification. For instance, more than 54% of cesium did not enter the (Ba,Cs,Cr)-hollandite tunnels. For (Ba,Cs,Ga)-hollandite, more than 37% of cesium did not enter the structure and a Cs-rich parasitic phase ($CsGaSi_{0.4}Ti_{0.6}O_4$) was detected both by SEM and ^{133}Cs MAS NMR. By analogy with $CsAlTiO_4$, this phase exhibited probably low chemical durability against water. The formation of a Cs-rich parasitic phase ($Cs(Al_{0.5}Ga_{0.5})TiO_4$) –analogous to that formed in (Ba,Cs,Ga)-hollandite – was also observed in the mixed (Ba,Cs,Al + Ga)-hollandite ceramic. Consequently, the low densification of ceramics and/or the occurrence of low durability Cs-rich parasitic phases precluded the use of (Ba,Cs,M)-hollandite ceramics ($M^{3+} = Al^{3+}$, Cr^{3+} and Ga^{3+}) prepared by oxide route at 1200 °C as waste forms for Cs immobilization.

(iv) (Ba,Cs,Fe)-hollandite was shown to retain all cesium in its structure. Significant amount of an iron-rich parasitic phase (Fe_2TiO_5) was detected but the occurrence of this phase – that did not concentrate cesium – is not a problem for the use of this ceramic as Cs waste form. Contrary to (Ba,Cs,M)-hollandite ceramics with aluminum, chromium or gallium, the introduction of cesium in (Ba,Cs,Fe)-hollandite has no consequence on ceramic porosity. Thus, introduction of Fe_2O_3 in powders mixture and of Fe^{3+} ions in site B has favorable effects on densification and Cs incorporation processes. This can be explained both by the relatively low Fe_2O_3 melting point (Table 4) and by the high size of Fe^{3+} ions in comparison with Al^{3+}, Cr^{3+} and Ga^{3+} ions (Table 1). The mixed (Ba,Cs,Al + Fe)-hollandite was also shown to retain almost all cesium (~90%). Iron-rich parasitic phase was not observed but, due to the occurrence of Al_2O_3, the porosity of the mixed ceramic sample is higher than the one of (Ba,Cs,Fe)-hollandite. The comparison of mixed (Ba,Cs,

Al + Fe)-hollandite ceramic synthesized by oxide route with a similar sample prepared by alkoxide route showed that a small proportion of cesium evaporated during sintering for the former method. The highest temperature used during calcination for the alkoxide route could explain this difference.

According to the high Cs retention, to the lack of Cs-rich parasitic phase of low lixiviation resistance and to their low porosity, (Ba,Cs,Fe)- and (Ba,Cs, Al + Fe)-hollandite ceramics prepared by oxide route can thus be envisaged as good candidates for radioactive cesium immobilization. Nevertheless, to complete this study, chemical durability tests have still to be performed to evaluate the capacity of these ceramics to retain Cs during lixiviation. As Zandbergen et al. [13] reported that rubidium can totally substitute cesium in $(Ba,Cs)(Ti,Al)_8O_{16}$ hollandite samples (the cation radius of Rb^+ and Cs^+ are, respectively, 1.61 and 1.74 Å in eightfold coordination [49]), we can expect that (Ba,Cs + Rb,Fe)- and (Ba,Cs + Rb,Al + Fe)-hollandite ceramics would simultaneously immobilize cesium and rubidium.

Acknowledgement

The CEA and the GDR Nomade are gratefully acknowledged for their financial support. We thank G. Leturcq (CEA Marcoule) for his help during the preparation of the hollandite sample by alkoxide route.

References

[1] W.E. Lee, M.I. Ojovan, M.C. Stennett, N.C. Hyatt, Adv. Ceram. 105 (2006) 3.
[2] M.I. Ojovan, W.E. Lee, An Introduction to Nuclear Waste Immobilization, Elsevier, 2005, p. 116.
[3] B. Boullis, Retraitement et séparation des radionucléides à vie longue, in: R. Turlay (Ed.), Les déchets nucléaires, Les Editions de Physique, France, 1997, p. 69.
[4] B. Boullis, Clefs CEA 53 (2006) 80.
[5] J.P. Coutures, C. Fillet, G. Blondiaux, L'Act. Chim. 285&286 (2005) 60.
[6] J-F. Dozol, V. Lamare, Clefs CEA 46 (2002) 28.
[7] J.P. Nabot, F. Sudreau, Clefs CEA 53 (2006) 89.
[8] N.J. Hess, F.J. Espinosa, S.D. Conradson, W.J. Weber, J. Nucl. Mater. 281 (2000) 22.
[9] R. Roy, E.R. Vance, Mater. Res. Bull 17 (1982) 585.
[10] S.E. Kesson, T.J. White, Proc. R. Soc. London A 405 (1986) 73.
[11] F. Bart, G. Leturcq, H. Rabiller, in: Environmental Issues and Waste Management Technologies in the Ceramic and Nuclear Industries IX: Proceedings of the symposium held at the 105th Annual Meeting of The American Ceramic Society, April 27–30, Nashville, Tennessee, Ceram. Trans. 155 (2004) 11.
[12] I. MacLaren, J. Cirre, C.B. Ponton, J. Am. Ceram. Soc 82 (1999) 3242.
[13] H.W. Zandbergen, P.L.A. Everstijn, F.C. Mijlhoff, G.H. Renes, D.J.W. Ijdo, Mater. Res. Bull 22 (1987) 431.
[14] Z. Asfari, C. Bressot, J. Vicens, C. Hill, J.F. Dozol, H. Rouquette, S. Eymard, V. Lamare, B. Tournois, Anal. Chem 67 (1995) 3133.
[15] A.E. Ringwood, S.E. Kesson, N.G. Ware, W.O. Hibberson, A. Major, Nature 278 (1979) 219.
[16] A.E. Ringwood, S.E. Kesson, N.G. Ware, W.O. Hibberson, A. Major, Geochem. J. 13 (1979) 141.
[17] A.E. Ringwood, S.E. Kesson, K.D. Reeve, D.M. Levins, E.J. Ramm, in: W. Lutze, R.C. Ewing (Eds.), Radioactive Waste Forms for the Future, North Holland, Amsterdam, 1988, p. 233.
[18] R.W. Cheary, Acta Crystallogr. B 42 (1986) 229.
[19] M.L. Carter, E.R. Vance, D.R.G. Mitchell, J.V. Hanna, Z. Zhang, E. Loi, J. Mater. Res. 17 (2002) 2578.
[20] V. Aubin, D. Caurant, D. Gourier, N. Baffier, T. Advocat, F. Bart, G. Leturcq, J-M. Costantini, Mater. Res. Soc. Symp. Proc. 807 (2004) 315.
[21] V. Aubin, D. Caurant, D. Gourier, N. Baffier, S. Esnouf, T. Advocat, Mater. Res. Soc. Symp. Proc. 792 (2004) 61.
[22] V. Aubin-Chevaldonnet, D. Gourier, D. Caurant, S. Esnouf, T. Charpentier, J.M. Costantini, J. Phys. Condens. Matter 18 (2006) 4007.
[23] V. Aubin-Chevaldonnet, PhD thesis, University Paris VI, France, 2004.
[24] R.W. Cheary, Acta Crystallogr. B 43 (1987) 28.
[25] K.R. Whittle, S.E. Ashbrook, S.A.T. Redfern, G.R. Lumpkin, J.P. Attfield, M. Dove, I. Farnan, Mater. Res. Soc. Symp. Proc. 807 (2004) 339.
[26] W. Sinclair, G.M. McLaughlin, A.E. Ringwood, Acta Crystallogr. B 36 (1980) 2913.
[27] R.W. Cheary, Mater. Sci. Forum 27&28 (1988) 397.
[28] E. Fanchon, PhD thesis, University of Grenoble, France, 1987.
[29] R.W. Cheary, R. Thompson, P. Watson, Mater. Sci. Forum 228–231 (1996) 777.
[30] V. Aubin-Chevaldonnet, P. Deniard, M. Evain, A.Y. Leinekugel-Le-Cocq-Errien, S. Jobic, D. Caurant, V. Petricek, T. Advocat, Z. Kristallogr, submitted for publication.
[31] S.E. Kesson, Radioact. Waste Manag. Nucl. Fuel Cycle 4 (1983) 53.
[32] J.S. Hartman, E.R. Vance, W.P. Power, J.V. Hanna, J. Mater. Res. 13 (1998) 22.
[33] J.M. Loezos, T.A. Vanderah, A.R. Drews, Powder Diffr. 14 (1999) 31.
[34] M.L. Cater, Mater. Res. Bull. 39 (2004) 1075.
[35] J.E. Post, R.B. Von Dreele, P.R. Buseck, Acta Crystallogr. B 38 (1982) 1056.
[36] J. Zhang, C.W. Burnham, Am. Mineral. 79 (1994) 168.
[37] R.W. Cheary, J. Kwiatkowska, J. Nucl. Mater. 125 (1984) 236.
[38] R.W. Cheary, R. Squadrito, Acta Crystallogr. A 48 (1992) 15.
[39] R.W. Cheary, R. Squadrito, Acta Crystallogr. B 45 (1989) 205.

[40] E. Fanchon, J.L. Hodeau, J. Vicat, J. Solid State Chem. 92 (1991) 88.
[41] S.E. Kesson, T.J. White, Proc. R. Soc. A 408 (1986) 295.
[42] A. Guinier, Théorie et technique de la radiocristallographie, Dunod, Paris, 1964.
[43] G. Leturcq, L. Lacroix-Orio, F. Bart, Conference Atalante 2004: Advances for Future Nuclear Fuel Cycles, Nîmes France, 21–24 June 2004.
[44] P. Boch, Matériaux et processus céramiques, Hermes Science Publications, Paris, 2001, p. 76.
[45] S.E. Kesson, T.J. White, J. Solid State Chem. 63 (1986) 122.
[46] B.M. Gatehouse, Acta Crystallogr. C 45 (1989) 1674.
[47] M.L. Carter, E.R. Vance, H. Li, in: Environmental Issues and Waste Management Technologies in the Ceramic and Nuclear Industries IX: Proceedings of the symposium held at the 105th Annual Meeting of The American Ceramic Society, April 27–30, Nashville, Tennessee, Ceram. Trans. 155 (2004) 21.
[48] K.R. Whittle, G.R. Lumpkin, S.E. Ashbrook, Mater. Res. Soc. Symp. Proc. 824 (2004) 243.
[49] R.D. Shannon, Acta Crystallogr. A 32 (1976) 751.
[50] F.C. Mijhloff, D.J.W. Ijdo, H.W. Zandbergen, Acta Crystallogr. B 41 (1985) 98.
[51] CRC Handbook of Chemistry and Physics, CRC Press, 1997–1998.